



This is a repository copy of *Natural selection and the predictability of evolution in Timemastick insects.*

White Rose Research Online URL for this paper:
<http://eprints.whiterose.ac.uk/127707/>

Version: Accepted Version

Article:

Nosil, P. orcid.org/0000-0002-8271-9005, Villoutreix, R. orcid.org/0000-0002-1815-3844, de Carvalho, C.F. orcid.org/0000-0002-5780-5454 et al. (5 more authors) (2018) Natural selection and the predictability of evolution in Timemastick insects. *Science*, 359 (6377). pp. 765-770.

<https://doi.org/10.1126/science.aap9125>

Reuse

Unless indicated otherwise, fulltext items are protected by copyright with all rights reserved. The copyright exception in section 29 of the Copyright, Designs and Patents Act 1988 allows the making of a single copy solely for the purpose of non-commercial research or private study within the limits of fair dealing. The publisher or other rights-holder may allow further reproduction and re-use of this version - refer to the White Rose Research Online record for this item. Where records identify the publisher as the copyright holder, users can verify any specific terms of use on the publisher's website.

Takedown

If you consider content in White Rose Research Online to be in breach of UK law, please notify us by emailing eprints@whiterose.ac.uk including the URL of the record and the reason for the withdrawal request.



eprints@whiterose.ac.uk
<https://eprints.whiterose.ac.uk/>

1 **Natural Selection And The Predictability Of Evolution In *Timema* Stick**

2 **Insects**

3

4 Patrik Nosil¹, Romain Villoutreix¹, Clarissa F. de Carvalho¹, Timothy E. Farkas², Víctor Soria-
5 Carrasco¹, Jeffrey L. Feder³, Bernard J. Crespi⁴, Zach Gompert⁵

6

7 ¹*Department of Animal and Plant Sciences, University of Sheffield, Sheffield, S10 2TN, UK*

8 ²*Department of Ecology and Evolutionary Biology, University of Connecticut, Storrs,*

9 *Connecticut 06369, USA*

10 ³*Department of Biological Sciences, University of Notre Dame, Notre Dame, Indiana 46556,*

11 *USA*

12 ⁴*Department of Biological Sciences, Simon Fraser University, Burnaby, BC V5A 1S6, Canada*

13 ⁵*Department of Biology, Utah State University, Logan, Utah 84322, USA*

14

15 **Predicting evolution remains difficult. We study the evolution of cryptic body coloration**
16 **and pattern in a stick insect using 25 years of field data, experiments, and genomics. We**
17 **find that evolution is more difficult to predict when it involves a balance between multiple**
18 **selective factors and uncertainty in environmental conditions than when it involves**
19 **feedback loops that cause consistent back and forth fluctuations. Specifically, changes in**
20 **color morph frequencies are modestly predictable through time ($r^2 = 0.14$), and driven by**
21 **complex selective regimes and yearly fluctuations in climate. In contrast, temporal changes**
22 **in pattern morph frequencies are highly predictable due to negative frequency-dependent**
23 **selection ($r^2 = 0.86$). For both traits, however, natural selection drives evolution around a**
24 **dynamic equilibrium, providing some predictability to the process.**

25

26 **Introduction:**

27

28 Evolutionary biology is often portrayed as a descriptive rather than predictive science (1, 2).

29 Nonetheless, the extent to which past evolution predicts future evolution can be quantified by

30 testing how well early subsets of a time series predict subsequent changes. However,

31 predictability in the form of such temporal autocorrelation does not consider the underlying

1 mechanisms driving evolutionary change, and thus can be inherently low. Considering the
2 mechanisms of evolution can lead to increased understanding of evolutionary change and its
3 predictability, and we study such mechanisms here.

4
5 Evolutionary predictability is mediated by several factors. First, evolution can be unpredictable
6 because of random processes, such as genetic drift (3). Second, even when evolution occurs by
7 deterministic natural selection, predictive power can be diminished if multiple, complex forms of
8 selection act simultaneously and by uncertainties in how the ecological conditions that affect
9 selection change through time (1, 2, 4-7). For example, negative frequency-dependent selection
10 (NFDS) favoring rare alleles can enhance predictability by causing increases in allele frequency
11 to be followed predictably by decreases (and *vice-versa*)(8, 9). However, the extent of
12 predictability will depend on how NFDS interacts with other evolutionary processes (e.g.,
13 directional selection stemming from climate change), and on whether the ecological conditions
14 that affect these other processes can themselves be predicted. Third, the interaction of genes
15 within their genomic context (i.e., dominance and epistasis) and with the environment (i.e.,
16 plasticity) may affect the anticipated trajectory of evolution (10-12). For example, directional
17 selection is expected to produce a predictable evolutionary response only if the traits affected are
18 reasonably heritable, and even then responses can be complex and nuanced (4-7, 10).

19
20 Studying the predictability of evolution across different timescales is particularly challenging (1,
21 2). For example, the immediate impact of natural selection can be readily measured in short-term
22 field studies or experiments. Such studies suggest that strong selection is not uncommon at the
23 scale of one or a few generations (13, 14), especially when new environments are colonized (15-
24 17). However, short-term changes need not translate into long-term directional trends. Rather,
25 evolution across geologic and phylogenetic time scales may be characterized by periods of
26 relative stasis interspersed between occasional bursts of sustained directional change, consistent
27 with Simpson's fossil-record inspired model of 'adaptive zones' (18, 19). Indeed, strong but
28 fluctuating selection can generate a pattern of little change when averaged over longer time
29 periods (14). Field studies that measure patterns of evolution over many years or decades are
30 somewhat intermediate between immediate and geologic time scales and thus have the potential
31 to illuminate how short-term selection relates to longer-term patterns of evolution (1, 20-22).

1 Such studies are rare because they require long-term temporal monitoring that cannot be sped up
2 with more effort. We here analyze the predictability of evolution in a long-term study of the stick
3 insect *Timema cristinae* (Fig. 1), and bolster our inferences using manipulative experiments and
4 genomic analyses.

6 **Polymorphism in stick insects**

8 *T. cristinae* is a univoltine, wingless, plant-feeding stick insect that exhibits three morphs that are
9 cryptic on different plant species or tissues (Figs. 1, 2)(23-27). A green morph bearing a white
10 dorsal stripe is cryptic on the leaves of *Adenostoma fasciculatum*, a green and unstriped morph is
11 cryptic on the leaves of *Ceanothus spinosus*, and a melanistic (i.e., brownish/grey and unstriped)
12 morph is cryptic on the stems of both hosts (but is conspicuous on leaves). Accordingly, the
13 striped morph is common on *Adenostoma*, the unstriped morph is common on *Ceanothus*, and
14 the melanistic morph is found at ~10% frequency on both hosts. We refer to the variation
15 between green (striped plus unstriped) and melanistic individuals as ‘color polymorphism’ and
16 that between green-striped and green-unstriped individuals as ‘pattern polymorphism’ (i.e., color
17 and pattern are different ‘traits’). These polymorphisms are highly heritable with strong genetic
18 dominance (melanistic body coloration is recessive to green and stripe pattern is recessive to
19 unstriped; details below)(23, 24).

21 Several processes maintain color and pattern polymorphism (23-27). A balance between
22 divergent selection and gene flow between populations on *Adenostoma* versus *Ceanothus* helps
23 maintain pattern polymorphism (26, 27). However, other factors likely contribute because even
24 areas dominated by one host rarely fix for a single pattern morph (26, 27). The frequency of
25 melanism does not vary markedly among populations such that variation in color is maintained
26 by balancing selection within populations, potentially involving heterozygote advantage and
27 selection that varies with microhabitat (stems versus leaves)(23, 24). Spatial and host-related
28 aspects of evolution for these morphs are thus reasonably well understood. In contrast, whether
29 and how morph frequencies change through time, and if they do so predictably, is unknown.

30 We studied temporal dynamics in *T. cristinae* using 25 years of field data from the mountains
31 around Santa Barbara, California (545 locality-by-host-by-year estimates of morph frequency on

1 the basis of 34,383 individuals collected from 1990 to 2017, mean n per locality-by-host-by-year
2 = 63, s.d. = 141, Database S1). We focus our autocorrelation analyses of predictability (28) on
3 the locality HV (an acronym for Hidden Valley), where we collected data over a continuous 18-
4 year period, with no years of missing data (total n = 3470, mean yearly n = 193, s.d. = 268).

5 **Results:**

6 **Temporal change in allele frequencies**

7
8 We tested the hypothesis that temporal change in allele frequencies at the genetic region
9 underlying the morphs is due, in part, to natural selection. Although past studies support
10 selection on the morphs (23-27), these results do not mean that all temporal changes are due to
11 selection, because selection and drift are not mutually exclusive (29, 30). Genomic data from
12 different time points provide a means to test for selection, because strongly selected regions are
13 expected to show greater change through time than the more neutral genomic background (29,
14 31). Genomic data are further required in our specific instance because genetic dominance and
15 heterozygote excess complicate inference of allele frequency change using phenotypic data alone
16 (23, 24).

17
18 We used *de novo* genome sequencing of a melanistic and green morph, with Dovetail hi-rise
19 scaffolding of Illumina reads (N50 = ~16 and 8 megabases, respectively)(32), linkage mapping
20 (25), and genome-wide association (GWA) mapping to explicitly delimit a single, contiguous
21 genomic region (~10.5 megabases in size) associated with color and pattern variation (Figs. 2,
22 S1-2). Consistent with a similar study with a more fragmented reference genome, this region
23 exhibits three core haplotypes (i.e., alleles), one corresponding to each morph, designated *s*, *u*,
24 and *m* for green-striped, green-unstriped, and melanistic, respectively (i.e., in terms of diploid
25 genotypes and phenotypes: *uu*, *us* and *um* = green-unstriped; *ss* and *sm* = green-striped; *mm* =
26 melanistic)(23). We refer to this region as the *Mel-Stripe* locus hereafter.

27
28 We quantified allele frequency changes at *Mel-Stripe* over time within three published data sets:
29 (1) genotyping-by-sequencing (GBS) data collected in a natural population on *Adenostoma*
30 (FHA, acronym for locality Far Hill on *Adenostoma*) in 2011 and 2013 (30, 33), (2) re-sequenced

1 whole genomes from individuals collected in FHA and used in an eight-day (i.e., within-
2 generation) release and recapture field experiment (30), and (3) GBS data in a between-year (i.e.,
3 between-generation) field transplant experiment (25).

4
5 In each case, we contrasted change through time at *Mel-Stripe* to that of the remainder of the
6 genome (to all genomic scaffolds, i.e., loci, that harbored as many single nucleotide
7 polymorphisms as *Mel-Stripe*, which was 40, 16, and 39 loci, respectively, for the data sets noted
8 above). Due to our explicit interest in *Mel-Stripe* we did not attempt to delimit other loci under
9 selection. If such loci exist they could upwardly bias our estimates of genome-wide change
10 relative to a case of neutrality, making our results for *Mel-Stripe* conservative.

11
12 We found that *Mel-Stripe* showed the greatest temporal allele frequency change of all genomic
13 regions, in all three data sets (FHA, change = 0.0273, $P = 0.024$; within-generation experiment,
14 change = 0.0340, $P = 0.059$; between-generation experiment, change = 0.0988, $P = 0.025$; exact
15 probabilities; Fisher's combined probability test across data sets: $X^2 = 20.50$, d.f. = 6, $P = 0.0023$,
16 Fig. 2). Dispersal alone is unlikely to drive these observed patterns because FHA was sampled
17 over an area that is larger ($>10,000 \text{ m}^2$) than the dispersal capacity of *T. cristinae* (i.e., one to a
18 few dozen meters per generation)(30, 33, 34). Furthermore, field surveys detected essentially no
19 dispersal off experimental bushes in the recapture study (30), and selection on pattern has been
20 previously observed in the presence, but not the absence of predation (with dispersal possible in
21 both treatments)(35, 36). Thus, selection likely contributed to the genetic change we observed at
22 the *Mel-Stripe* locus. We thus next turned to whether such selection was associated with weakly
23 or strongly predictable patterns of evolution.

24

25 **Predictability of the evolution of body color and complex selection regimes**

26

27 We quantified the predictability of evolution using autoregressive moving average models,
28 ARMA (28). This analysis revealed that that color morphs at Hidden Valley (HV) exhibited
29 subtle and only moderately predictable changes through time (median predictive $r^2 = 0.14$,
30 ARMA, Fig. 3, Table S1). This was associated with support for multiple, complex, and
31 counteracting sources of selection (Fig. 4). Across the 25-year study period, the frequency of

1 melanistic morphs increased in years where spring temperatures were warmer (overall effect of
2 temperature = 0.187, 95% equal-tail probability intervals = 0.063-0.309; correlation between
3 observed and predicted frequency from cross-validation = 0.16, 95% CI = 0.04-0.28, $P = 0.0102$,
4 Bayesian hierarchical linear model, Fig. 4, Table S2). However, lab experiments indicate that
5 melanistic individuals have weaker heat tolerance, relative to green individuals ($B = 3.57$, 95%
6 CIs = 1.34-9.51, $P = 0.0111$, Cox proportional hazards regression model using exact likelihood).
7 These results imply that selection for crypsis on dry, brownish plants in warmer years may favor
8 dark colors, but that thermoregulatory selection acts in an opposing direction. However, further
9 work is required to test this hypothesis directly, and to establish how well the laboratory
10 experiments match field conditions. Notably, melanistic individuals exhibit fewer fungal
11 infections and greater mating success than other morphs, further suggesting that selection is
12 multi-faceted (24).

13

14 Given selection appears complex, we used our genomic data to estimate selection coefficients
15 explicitly (for all six diploid genotypes underlying the morphs, with three alleles: s , m , and u).
16 This analysis revealed that viability selection on *Adenostoma* during late life-history stages (i.e.,
17 in the within-generation experiment) favored the s/s homozygote (posterior probability that
18 fitness of $s/s >$ than the following genotypes: $m/u = 0.93$, $u/u = 0.81$, $m/m = 0.82$, $m/s = 0.84$, u/s
19 $= 0.91$). In contrast, the most-fit genotype between years at the FHA locality (also on
20 *Adenostoma*) was the s/m heterozygote (posterior probability that fitness of $s/m >$ than the
21 following genotypes: $m/u = 0.90$, $s/s = 0.97$, $u/u = 0.81$, $m/m = 0.92$, $u/s = 0.94$). Both s/s and s/m
22 are green-striped in terms of phenotype, and cryptic on *Adenostoma*. Thus, a fluctuating balance
23 between many factors, potentially including heterozygote advantage (23), may explain why
24 evolution involving the deterministic process of selection was not more highly predictable.

25

26 **Predictability of the evolution of pattern**

27

28 Our findings for color raise the question of whether evolution is ever highly predictable? We
29 address this issue by re-analyzing the data from Hidden Valley (HV) considering striped versus
30 unstriped individuals (i.e., pattern, rather than color, polymorphism). This demonstrates that
31 striped morph frequencies at HV exhibited consistent increases followed by decreases (i.e., up

1 and down fluctuations) across 18 consecutive years (Binomial sampling probability < 0.0001 ,
2 Fig. 3). Thus, the evolution of pattern was highly predictable (median predictive $r^2 = 0.86$,
3 ARMA). In fact, predictive power at the scale of three to five years was near perfect (>0.95), and
4 remained high even after a decade (>0.80). The observed pattern of predictable of up and down
5 fluctuations could reflect a case where predators have specific search images for common prey,
6 resulting in NFDS selection favoring rare prey phenotypes.

7

8 **Morph frequency and selection**

9

10 To test the NFDS hypothesis, we transplanted green-striped and green-unstriped *T. cristinae* to
11 *Adenostoma* in either 1:4 or 4:1 ratios ($n = 1000$ individuals, 10 replicates per treatment, Fig. 5).
12 The NFDS hypothesis predicts that the striped morph, cryptic on *Adenostoma*, would exhibit a
13 stronger survival advantage when rare. Supporting this prediction, the striped morph experienced
14 strong selection when initially rare (selection coefficient, $s = 0.70$), and increased in frequency in
15 all 10 experimental replicates (posterior probability that change > 0 was >0.999). In contrast, the
16 striped morph showed idiosyncratic changes when initially common ($s = -0.04$, posterior
17 probability that change $> 0 = 0.43$). Although our results differ from NFDS where the sign of
18 selection reverses very strongly, they are consistent with the strength of selection being
19 dependent on frequency (i.e., directional selection that weakens with increasing allele frequency
20 is akin to frequency-dependent selection). It is possible that selection against the striped morph
21 would be more strongly negative if ratios were manipulated more extremely (e.g., to 10:1).

22 **Conclusions:**

23

24 We observed complex and fluctuating sources of selection. Together with gene flow (26), these
25 selection pressures likely contribute to relative stability in the difference between hosts in morph
26 frequency over the 25-year study period (Fig. 5). Complex and fluctuating selection may thus
27 help maintain polymorphism, but prevent divergence of sufficient magnitude to strongly drive
28 speciation (24). NFDS in particular may cause evolutionary systems to exhibit resilience, as
29 reported in other complex ecological, social, and physical systems (37-39). Such resilience
30 increases predictability of short-term evolution, because a system returns to its former state
31 following perturbation. However, it can make long-term predictions difficult because substantial

1 evolution only happens when the system reaches a tipping point that pushes it more permanently
2 to a very different state.

3 Finally, our results suggest that the predictability of evolution can depend on the nature of
4 selection, and our understanding of it. Thus, we predicted evolution more accurately for pattern,
5 where selection appears to be strongly associated with frequency, than for color, where a myriad
6 of factors, some poorly understood, affect fitness. As further illustration of this point,
7 predictability in the form of temporal autocorrelation is modest to weak in other well-known
8 studies of contemporary evolution: beak and body size changes in Darwin's finches and morph
9 frequency changes in the scarlet tiger and peppered moth(21, 40, 41)(median predictive power
10 per study system, r^2 , in 3-10 year forecasting analyses 0.03-0.18, ARMA, Figs 6, S3-S6, Table
11 S1). Adding climatic (i.e., rainfall) data to the *Geospiza* finch case, where climate is known to
12 affect seed distributions, improves predictive power in *Geospiza fortis* (e.g., mean r^2 increase
13 relative to a model without rainfall = 0.08, ARMA; Table S3). Nonetheless, predictive power
14 even considering rainfall is modest and increased only in one of the two finch species examined
15 (Table S3). It is possible that predictability remains limited because seed size itself was not
16 modeled, because the relationship between evolution and rainfall is complex such that only
17 extreme droughts have strong effects, and because some extreme climatic events precede the ten-
18 year period that our forecasting is based upon.

19
20 In conclusion, our constrained understanding of selection and environmental variation (i.e.,
21 limits on data and analysis), rather than inherent randomness, can thus limit ability to predict
22 evolution. In turn, these limitations may affect our understanding of ecological processes,
23 because to the extent that evolution can be predicted, perhaps so can its ecological consequences
24 for population dynamics, community structure, and ecosystem functioning (42-44).

25 26 **Acknowledgements**

27
28 The work was funded by a grant from the European Research Council (NatHisGen R/129639) to
29 P. Nosil and a Natural Sciences and Engineering Research Council grant to B.J. Crespi (NSERC
30 06505). V. Soria-Carrasco was supported by a Leverhulme Trust Early Career Fellowship. We
31 thank C. Sandoval for contributing data on morph frequencies. C. Sandoval, A. Comeault, M.

1 Muschick, R. Riesch, and T. Reimchen provided discussion and comments on previous versions
 2 of the manuscript. The support and resources from the Center for High Performance Computing
 3 at the University of Utah are gratefully acknowledged, as well as access to the High Performance
 4 Computing Facilities, particularly to the Iceberg HPC cluster, from the Corporate Information
 5 and Computing Services at the University of Sheffield. The genome drafts reported in this paper
 6 have been deposited in the Genomes database of the National Center for Biotechnology
 7 Information (NCBI) under BioProject Accession PRJNA417530. Other data, including custom
 8 code written for analyses, have been archived in Dryad Digital Repository XXXX (number can
 9 only be provided by Dryad if the manuscript is accepted). Rosa Ribas drew all the figures.

11 **Author contributions**

13 PN and ZG conceived the project. PN, RV, CC, TEF, VS, ZG contributed data and analyses. PN,
 14 JLF, and ZG wrote the manuscript, with feedback from all authors.

16 **Figure 1.** Drawings of the three morphs of *T. cristinae*.

18 **Figure 2.** Genomic change through time at the *Mel-Stripe* locus. (a) Manhattan plots showing
 19 results for genome-wide association mapping of color. The y-axes show *P*-values, with red
 20 denoting genome-wide significance. The left-land plot shows results genome wide (LG = linkage
 21 group). The right-hand plot is zoomed in on LG8, which shows the bulk of association, and here
 22 numbers below the x-axis delimit different genomic scaffolds. The *Mel-Stripe* locus is evident by
 23 the block of strong association spanning scaffolds 702.1 and 128. (b) Allele-frequency change
 24 through time in the natural population FHA (2011 versus 2013). (c) Allele-frequency change
 25 through time in the within-generation experiment. (d) Allele-frequency change through time in
 26 the between-generation experiment. In panels b-d the vertical red line shows change at the *Mel-*
 27 *Stripe* locus and the histogram shows the distribution of change across other similar-sized
 28 scaffolds in the genome (i.e., the genomic background).

30 **Figure 3.** Predicting evolution in *Timema cristinae* stick insects. (a) Schematic of analytical
 31 approach for predicting evolution using temporal autocorrelation. Black points represent

1 observed values in a time series. Some number of these observed points are removed (in this case
 2 the six right-hand most points) and the missing values for them are predicted using the remainder
 3 of observed points. Predictive power is the strength of association between observed and
 4 predicted values. (b) Color morph frequencies through time. (c) Pattern morph frequencies
 5 through time. (d) Change in color morph frequencies. (e) Change in pattern morph frequencies.
 6 (f) Predicting change in color morph frequencies (r^2). (g) Predicting change in pattern morph
 7 frequencies (r^2). (h) Predicting change in color morph frequencies (r). The difference from panel
 8 (f) is that r -values are not squared such that their sign is evident. Shaded areas are 95%
 9 confidence intervals. (i) Predicting change in pattern morph frequencies (r). The difference from
 10 panel (g) is that r -values are not squared such that their sign is evident. Shaded areas are 95%
 11 confidence intervals.

12

13 **Figure 4.** Complex patterns of natural selection. (a) Associations between the frequency of
 14 melanistic morphs and yearly spring temperature. Positive effects indicate increases in melanistic
 15 frequency with increased temperature. Significant effects are shown in red. The left-most data
 16 point represents the average effect across populations, and the remaining points are for individual
 17 populations. Note that among-population variation is high, but that all significant effects are
 18 positive. (b) Morph-specific survival time in thermoregulatory (i.e., heat tolerance) lab
 19 experiments. (c) Genotype specific fitness in the within-generation experiment on the host
 20 *Adenostoma* (*s/s* is most fit). Shown are the posterior probabilities from estimates of genotype-
 21 specific fitness. (d) Genotype specific fitness in the natural population FHA on *Adenostoma* (*s/m*
 22 is most fit). Shown are the posterior probabilities from estimates of genotype-specific fitness.

23

24 **Figure 5.** Evidence for negative-frequency dependent selection on pattern, and resulting stability
 25 in morph frequency differences between hosts. (a) Posterior probability estimates of the selection
 26 coefficient in each treatment. Positive values on the x-axis represent selection favoring striped
 27 individuals. (b) Changes in the frequency of striped morphs in releases at 20% of the population
 28 and 80% of the population during the course of the experiment. (c) Posterior probability
 29 distributions of change in the frequency of striped morph per treatment. (d) Yearly differences
 30 between host plant species in natural populations in the frequency of striped morphs (lines
 31 denote posterior medians and shaded regions given the 95% equal-tail probability intervals).

1

2 **Figure 6.** Predicting evolution in different systems. (a) Predicting evolution for evolutionary
 3 time series in (left to right) *Geospiza fortis* body size, *Geospiza fortis* beak morphology
 4 (principle components 1 and 2), *G. scandens* body size, *G. scandens* beak morphology (principle
 5 components 1 and 2), *Panaxia dominula* and *Biston betularia* morph frequencies, and *T.*
 6 *cristinae* color and pattern morph frequencies. Boxplots show the distribution of r^2 between true
 7 and predicted evolutionary change across 3 to 10 year model-based forecasts. (b) Predicting
 8 evolution in studies (r). The difference from panel (a) is that r-values are not squared such that
 9 their sign is evident.

10

11 **References**

12

- 13 1. P. R. Grant, B. R. Grant, Unpredictable evolution in a 30-year study of Darwin's finches.
 14 *Science* **296**, 707-711 (2002).
- 15 2. M. Lässig, V. Mustonen, A. M. Walczak, Predicting evolution. *Nature Ecology &*
 16 *Evolution* **1**, 0077 doi:0010.1038/s41559-41017-40077 (2017).
- 17 3. D. L. Hartl, A. G. Clark, *Principles of population genetics, fourth edition.* (Sinauer,
 18 2007).
- 19 4. A. Ozgul, S. Tuljapurkar, T. G. Benton, J. M. Pemberton, T. H. Clutton-Brock, T.
 20 Coulson, The Dynamics of Phenotypic Change and the Shrinking Sheep of St. Kilda.
 21 *Science* **325**, 464-467 (2009).
- 22 5. T. Coulson, D. R. MacNulty, D. R. Stahler, B. Vonholdt, R. K. Wayne, D. W. Smith,
 23 Modeling Effects of Environmental Change on Wolf Population Dynamics, Trait
 24 Evolution, and Life History. *Science* **334**, 1275-1278 (2011).
- 25 6. J. Merila, Evolution in response to climate change: In pursuit of the missing evidence.
 26 *Bioessays* **34**, 811-818 (2012).
- 27 7. M. Bosse, L. G. Spurgin, V. N. Laine, E. F. Cole, J. A. Firth, P. Gienapp, A. G. Gosler,
 28 K. McMahon, J. Poissant, I. Verhagen, M. A. M. Groenen, K. van Oers, B. C. Sheldon,
 29 M. E. Visser, J. Slate, Recent natural selection causes adaptive evolution of an avian
 30 polygenic trait. *Science* **358**, 365-368 (2017).

- 1 8. M. Chouteau, V. Llaurens, F. Piron-Prunier, M. Joron, Polymorphism at a mimicry
2 supergene maintained by opposing frequency-dependent selection pressures. *Proc. Natl.*
3 *Acad. Sci. U. S. A.* **114**, 8325-8329 (2017).
- 4 9. D. I. Bolnick, W. E. Stutz, Frequency dependence limits divergent evolution by favouring
5 rare immigrants over residents. *Nature* **546**, 285-+ (2017).
- 6 10. R. Lande, Quantitative genetic analysis of multivariate evolution, applied to brain-body
7 size allometry. *Evolution* **33**, 402-416 (1979).
- 8 11. C. Rueffler, T. J. M. Van Dooren, O. Leimar, P. A. Abrams, Disruptive selection and
9 then what? *Trends Ecol. Evol.* **21**, 238-245 (2006).
- 10 12. X. Thibert-Plante, A. P. Hendry, The consequences of phenotypic plasticity for
11 ecological speciation. *J. Evol. Biol.* **24**, 326-342 (2011).
- 12 13. J. G. Kingsolver, H. E. Hoekstra, J. M. Hoekstra, D. Berrigan, S. N. Vignieri, C. E. Hill,
13 A. Hoang, P. Gibert, P. Beerli, The strength of phenotypic selection in natural
14 populations. *Am. Nat.* **157**, 245-261 (2001).
- 15 14. G. Bell, Fluctuating selection: the perpetual renewal of adaptation in variable
16 environments. *Philos. Trans. R. Soc. B-Biol. Sci.* **365**, 87-97 (2010).
- 17 15. P. F. Colosimo, K. E. Hosemann, S. Balabhadra, G. Villarreal, M. Dickson, J. Grimwood,
18 J. Schmutz, R. M. Myers, D. Schluter, D. M. Kingsley, Widespread parallel evolution in
19 sticklebacks by repeated fixation of ectodysplasin alleles. *Science* **307**, 1928-1933
20 (2005).
- 21 16. S. M. Rogers, P. Tamkee, B. Summers, S. Balabhadra, M. Marks, D. M. Kingsley, D.
22 Schluter, GENETIC SIGNATURE OF ADAPTIVE PEAK SHIFT IN THREESPINE
23 STICKLEBACK. *Evolution* **66**, 2439-2450 (2012).
- 24 17. C. Heliconius Genome, Butterfly genome reveals promiscuous exchange of mimicry
25 adaptations among species. *Nature* **487**, 94-98 (2012); published online Epub2012-Jul-5 (
26 18. G. G. Simpson, *Tempo and mode in evolution*. (Columbia University Press, New York,
27 1944).
- 28 19. G. G. Simpson, *The major features of evolution*. (Columbia University Press, New York,
29 1953).
- 30 20. A. M. Siepielski, J. D. DiBattista, S. M. Carlson, It's about time: the temporal dynamics
31 of phenotypic selection in the wild. *Ecol. Lett.* **12**, 1261-1276 (2009).

- 1 21. P. R. Grant, B. R. Grant, *40 Years of Evolution: Darwin's Finches on Daphne Major*
2 *Island*. (Princeton University Press, Princeton, 2014).
- 3 22. T. Dobzhansky, *Genetics and the Origin of Species*. (Columbia University Press, New
4 York, NY, ed. 3rd, 1951), pp. 364.
- 5 23. D. Lindtke, K. Lucek, V. Soria-Carrasco, R. Villoutreix, T. E. Farkas, R. Riesch, S. R.
6 Dennis, Z. Gompert, P. Nosil, Long-term balancing selection on chromosomal variants
7 associated with crypsis in a stick insect. *Mol. Ecol.* **26**, 6189-6205 (2017).
- 8 24. A. A. Comeault, S. M. Flaxman, R. Riesch, E. Curran, V. Soria-Carrasco, Z. Gompert, T.
9 E. Farkas, M. Muschick, T. L. Parchman, T. Schwander, J. Slate, P. Nosil, Selection on a
10 Genetic Polymorphism Counteracts Ecological Speciation in a Stick Insect. *Current*
11 *Biology* **25**, 1-7 (2015).
- 12 25. V. Soria-Carrasco, Z. Gompert, A. A. Comeault, T. E. Farkas, T. L. Parchman, J. S.
13 Johnston, C. A. Buerkle, J. L. Feder, J. Bast, T. Schwander, S. P. Egan, B. J. Crespi, P.
14 Nosil, Stick Insect Genomes Reveal Natural Selection's Role in Parallel Speciation.
15 *Science* **344**, 738-742 (2014).
- 16 26. C. P. Sandoval, The effects of relative geographical scales of gene flow and selection on
17 morph frequencies in the walking-stick *Timema cristinae*. *Evolution* **48**, 1866-1879
18 (1994).
- 19 27. P. Nosil, Divergent host plant adaptation and reproductive isolation between ecotypes of
20 *Timema cristinae* walking sticks. *Am. Nat.* **169**, 151-162 (2007).
- 21 28. N. Cressie, C. K. Wikle, *Statistics for Spatio-Temporal Data*. (John Wiley and Sons,
22 2011).
- 23 29. Z. Gompert, Bayesian inference of selection in a heterogeneous environment from
24 genetic time-series data. *Mol. Ecol.* **25**, 121-134 (2016).
- 25 30. Z. Gompert, A. A. Comeault, T. E. Farkas, J. L. Feder, T. L. Parchman, C. A. Buerkle, P.
26 Nosil, Experimental evidence for ecological selection on genome variation in the wild.
27 *Ecol. Lett.* **17**, 369-379 (2014).
- 28 31. M. Foll, H. Shim, J. D. Jensen, WFABC: a Wright-Fisher ABC-based approach for
29 inferring effective population sizes and selection coefficients from time-sampled data.
30 *Molecular ecology resources* **15**, 87-98 (2015).

- 1 32. N. H. Putnam, B. L. O'Connell, J. C. Stites, B. J. Rice, M. Blanchette, R. Calef, C. J.
2 Troll, A. Fields, P. D. Hartley, C. W. Sugnet, D. Haussler, D. S. Rokhsar, R. E. Green,
3 Chromosome-scale shotgun assembly using an in vitro method for long-range linkage.
4 *Genome Research* **26**, 342-350 (2016).
- 5 33. R. Riesch, M. Muschick, D. Lindtke, R. Villoutreix, A. A. Comeault, T. E. Farkas, K.
6 Lucek, E. Hellen, V. Soria-Carrasco, S. R. Dennis, C. F. de Carvalho, R. J. Safran, C. P.
7 Sandoval, J. L. Feder, R. Gries, B. J. Crespi, G. Gries, Z. Gompert, P. Nosil, Transitions
8 between phases of genomic differentiation during stick-insect speciation. *Nature Ecology*
9 *and Evolution* **1**, 0082 (2017).
- 10 34. C. Sandoval, Persistence of a walking-stick population (Phasmatoptera : Timematodea)
11 after a wildfire. *Southwestern Naturalist* **45**, 123-127 (2000).
- 12 35. P. Nosil, Reproductive isolation caused by visual predation on migrants between
13 divergent environments. *Proc. R. Soc. B-Biol. Sci.* **271**, 1521-1528 (2004).
- 14 36. P. Nosil, B. J. Crespi, Experimental evidence that predation promotes divergence in
15 adaptive radiation. *Proc. Natl. Acad. Sci. U. S. A.* **103**, 9090-9095 (2006).
- 16 37. M. Scheffer, S. R. Carpenter, T. M. Lenton, J. Bascompte, W. Brock, V. Dakos, J. van de
17 Koppel, I. A. van de Leemput, S. A. Levin, E. H. van Nes, M. Pascual, J. Vandermeer,
18 Anticipating Critical Transitions. *Science* **338**, 344-348 (2012).
- 19 38. M. Scheffer, S. Carpenter, J. A. Foley, C. Folke, B. Walker, Catastrophic shifts in
20 ecosystems. *Nature* **413**, 591-596 (2001).
- 21 39. P. Nosil, J. L. Feder, S. M. Flaxman, Z. Gompert, Tipping points in the dynamics of
22 speciation. *Nature Ecology and Evolution* **1**, 0001 (doi:0010.1038/s41559-41016-40001)
23 (2017).
- 24 40. L. M. Cook, D. A. Jones, The medionigra gene in the moth *Panaxia dominula*: The case
25 for selection. *Philos. Trans. R. Soc. Lond. Ser. B-Biol. Sci.* **351**, 1623-1634 (1996).
- 26 41. L. M. Cook, S. L. Sutton, T. J. Crawford, Melanic moth frequencies in Yorkshire, an old
27 English industrial hot spot. *Journal of Heredity* **96**, 522-528 (2005).
- 28 42. A. P. Hendry, *Eco-evolutionary dynamics*. (Princeton University Press, Princeton, New
29 Jersey, 2017).
- 30 43. T. W. Schoener, The Newest Synthesis: Understanding the Interplay of Evolutionary and
31 Ecological Dynamics. *Science* **331**, 426-429 (2011).

- 1 44. T. E. Farkas, T. Mononen, A. A. Comeault, I. Hanski, P. Nosil, Evolution of Camouflage
2 Drives Rapid Ecological Change in an Insect Community. *Current Biology* **23**, 1835-
3 1843 (2013).

4

5 **Supplementary References**

6

- 7 45. B. Langmead, S. L. Salzberg, Fast gapped-read alignment with Bowtie 2. *Nature*
8 *Methods* **9**, 357-U354 (2012).
- 9 46. H. Li, B. Handsaker, A. Wysoker, T. Fennell, J. Ruan, N. Homer, G. Marth, G. Abecasis,
10 R. Durbin, The Sequence Alignment/Map format and SAMtools. *Bioinformatics* **25**,
11 2078-2079 (2009).
- 12 47. Z. Gompert, L. K. Lucas, C. C. Nice, C. A. Buerkle, GENOME DIVERGENCE AND
13 THE GENETIC ARCHITECTURE OF BARRIERS TO GENE FLOW BETWEEN
14 LYCAEIDES IDAS AND L-MELISSA. *Evolution* **67**, 2498-2514 (2013).
- 15 48. Y. S. Aulchenko, S. Ripke, A. Isaacs, C. M. Van Duijn, GenABEL: an R library for
16 genome-wide association analysis. *Bioinformatics* **23**, 1294-1296 (2007).
- 17 49. A. L. Price, N. J. Patterson, R. M. Plenge, M. E. Weinblatt, N. A. Shadick, D. Reich,
18 Principal components analysis corrects for stratification in genome-wide association
19 studies. *Nature Genetics* **38**, 904-909 (2006).
- 20 50. P. Rastas, F. C. F. Calboli, B. C. Guo, T. Shikano, J. Merila, Construction of Ultradense
21 Linkage Maps with Lep-MAP2: Stickleback F-2 Recombinant Crosses as an Example.
22 *Genome Biology and Evolution* **8**, 78-93 (2016).
- 23 51. H. Li, R. Durbin, Fast and accurate short read alignment with Burrows-Wheeler
24 transform. *Bioinformatics* **25**, 1754-1760 (2009).
- 25 52. T. Schwander, B. J. Crespi, Multiple Direct Transitions from Sexual Reproduction to
26 Apomictic Parthenogenesis in Timema Stick Insects. *Evolution* **63**, 84-103 (2009).
- 27 53. S. V. Angiuoli, S. L. Salzberg, Mugsy: fast multiple alignment of closely related whole
28 genomes. *Bioinformatics* **27**, 334-342 (2011).
- 29 54. A. McKenna, M. Hanna, E. Banks, A. Sivachenko, K. Cibulskis, A. Kernytzsky, K.
30 Garimella, D. Altshuler, S. Gabriel, M. Daly, M. A. DePristo, The Genome Analysis

- 1 Toolkit: A MapReduce framework for analyzing next-generation DNA sequencing data.
2 *Genome Research* **20**, 1297-1303 (2010).
- 3 55. Z. Gompert, J. P. Jahner, C. F. Scholl, J. S. Wilson, L. K. Lucas, V. Soria-Carrasco, J. A.
4 Fordyce, C. C. Nice, C. A. Buerkle, M. L. Forister, The evolution of novel host use is
5 unlikely to be constrained by trade-offs or a lack of genetic variation. *Mol. Ecol.* **24**,
6 2777-2793 (2015).
- 7 56. O. J. T. Briet, P. H. Amerasinghe, P. Vounatsou, Generalized Seasonal Autoregressive
8 Integrated Moving Average Models for Count Data with Application to Malaria Time
9 Series with Low Case Numbers. *PLoS One* **8**, (2013).
- 10 57. M. C. Jones, Randomly choosing parameters from the stationary and invertibility region
11 of autoregressive-moving average models. *Applied Statistics* **36**, 134–138 (1987).
- 12 58. C. P. Sandoval, Differential Visual Predation on Morphs of *Timema*-*Cristinae*
13 (*Phasmatodeae*, *Timemidae*) and Its Consequences for Host-Range. *Biol. J. Linnean Soc.*
14 **52**, 341-356 (1994).
- 15 59. Q. D. Team, **QGIS Geographic Information System. Open Source, Geospatial**
16 **Foundation Project.** <http://www.qgis.org/>. (2016).
- 17 60. T. Therneau, P. Grambsch, *Modeling Survival Data: Extending the Cox Model*. Springer-
18 Verlag (2000).
- 19 61. T. Therneau. A Package for Survival Analysis in S. version, 2.38, <URL:
20 <http://CRAN.R-project.org/package=survival>>. (2015).
- 21 62. R. D. C. Team. (Vienna, Austria, 2013).
- 22 63. Z. Gompert, F. J. Messina, Genomic evidence that resource-based trade-offs limit host-
23 range expansion in a seed beetle. *Evolution* **70**, 1249-1264 (2016).
- 24
25



1
2
3
4 Supplementary Materials for

5
6 **Natural Selection And The Predictability Of Evolution In *Timema* Stick**
7 **Insects**

8
9 Patrik Nosil, Romain Villoutreix, Clarissa F. de Carvalho, Timothy E. Farkas, Víctor Soria-
10 Carrasco, Jeffrey L. Feder, Bernard J. Crespi, Zach Gompert

11
12 correspondence to: p.nosil@sheffield.ac.uk and zach.gompert@usu.edu

13
14
15 **This PDF file includes:**

16 Materials and Methods
17 Figs. S1 to S6
18 Tables S1 to S3
19 Caption for database S1

20
21
22 **Other Supplementary Materials for this manuscript includes the following:**

23 Database S1 [Raw population data]
24
25
26
27
28

1 **Materials and Methods**

3 Approach for delimiting the genetic region affecting color and color-pattern

5 Previous work showed that each morph in *T. cristinae* is a chromosomal form underlain by
6 a haplotype on a single linkage group (LG8), with restricted recombination between
7 chromosomal forms (23, 24). However, it relied on a fragmented reference genome such that it
8 could not delimit a single, contiguous region (i.e., locus) underlying each morph. We here
9 delimit the locus underlying the morphs and quantify its change through time relative to the rest
10 of the genome.

11
12 To do so, we generated higher-quality reference genomes for a melanistic and a green
13 morph of *T. cristinae* using Dovetail hi-rise scaffolding of Illumina reads (N50 = ~16, 8
14 megabases, respectively)(32). Comparison of the reference genomes, linkage mapping (25), and
15 genome-wide association (GWA) mapping allowed us to explicitly delimit a single, contiguous
16 genomic region associated with color and pattern variation (Figure 2, S1, S2). Accordingly, this
17 region exhibits three core haplotypes (i.e., alleles), one corresponding to each morph (with
18 melanistic recessive to green body coloration and stripe recessive to unstriped pattern), and we
19 refer to it as the *Mel-Stripe* locus hereafter. Details are contained below.

21 Reference genome with Dovetail

22
23 We generated reference genomes for a melanistic and a green morph using Dovetail
24 technology (32). For the melanistic morph we used two sequencing runs. The first run (short
25 reads + Chicago library) was done on a melanistic female from FHA caught in 2015 (id:
26 15_0190). The second run (Chicago library only) was done using another melanistic female
27 caught in 2016 in FHA (id 16_0359). For the green reference (short reads + Chicago libraries), a
28 green unstriped female from population PRC caught in 2015 was used (id 15_0802). The 2015
29 samples were flash frozen in liquid nitrogen, shipped to Sheffield and stored in a -80°C freezer.
30 It was de-gutted prior to shipping to Dovetail. The 2016 sample was caught and degutted ‘fresh’
31 in California and sent directly to Dovetail.

32
33 The Dovetail assembly method relies on building a conventional reference assembly using
34 Meraculous with paired-end Illumina reads and then using Chicago libraries for scaffolding
35 using the HiRise pipeline (32). Chicago libraries are produced by reconstituting chromatin *in*
36 *vitro* with chaperones and histones, followed by crosslinking (i.e. DNA stabilization by creating
37 covalent bonds among the histones), digestion with restriction enzymes, and ligation. This
38 process results in many chimeric fragments composed from physically distant regions, but
39 ensures they come from the same stabilized large fragment. In theory, the read pairs produced
40 can have separations up to the maximum fragment size of the DNA. A model of insert
41 distribution derived from the distances among the original fragments is then used for scaffolding.

42
43 The assembly based on melanistic females (draft 1.3) had a 63.0x sequencing depth with a
44 total length of 953.3 Mb (73.3% of the estimated genome size by flow cytometry)(25). It
45 comprised 4068 scaffolds (N50=16.4 Mb, N90=1.1 Mb, L50=16, L90=135), a significant

1 improvement relative to the previous draft 0.3 (14,221 scaffolds, N50=312.5 Kb, N90=52 Kb,
 2 L50=788, L90=3869; DDBJ/ENA/GenBank accession MSSY00000000.3)(33). We clustered
 3 scaffolds in major linkage groups as described in detail below in the section on delimitation of
 4 the *Mel-Stripe* locus, resulting in draft 1.3c2. This Whole Genome Shotgun project was
 5 deposited at DDBJ/ENA/GenBank under the accession PGFK00000000. The version described
 6 in this paper is version PGFK01000000. The assembly based on the green female had a 42.7x
 7 sequencing depth with a total length of 932.1Mb (71.1% of the estimated size). This assembly
 8 was poorer than the 1.3, but still significantly better than the previous 0.3 (5653 scaffolds,
 9 N50=8.2 Mb, N90=503.2 Kb, L50=22, L90=222). This assembly was labeled as draft 2.1. This
 10 Whole Genome Shotgun project was deposited at DDBJ/ENA/GenBank under the accession
 11 PGTA00000000. The version described in this paper is version PGTA01000000.

12

13 Genome-wide association (GWA) mapping

14

15 We mapped color and pattern variation using previously published GBS data (33) aligned to
 16 the new reference genome 1.3b2. We aligned 96.1% (789,388,267) of reads from 602 individuals
 17 using BOWTIE 2.2.9 (45) with the '--very-sensitive-local' preset. We used SAMTOOLS 1.3.1 (46)
 18 to sort and index the alignments. We used aligned reads with a mapping quality score of at least
 19 20 to call single nucleotide polymorphisms (SNPs) with SAMTOOLS mpileup and BCFTOOLS
 20 1.3.1 (46), using the original consensus caller (-c) with a P-value threshold of 0.05. From the
 21 1,369,070 variants called, we excluded those with quality score of less than 20, sampling
 22 coverage of less than 50%, maximum depth more than 10 times the number of total, minor-allele
 23 frequency (MAF) equal or less than 0.01, and more than two alleles. The number of phenotyped
 24 individuals was different for color (590) and pattern (536) and we subsequently subset variants
 25 and applied filters relative to the respective number of samples. Thus, we retained 418,209 bi-
 26 allelic variants for color and 416,405 variants for pattern. Both datasets were very similar,
 27 showing the same mean coverage depth per SNP per individual of 5.1x (95%: 0-15; per SNP
 28 average: 5.1x, 95%: 1.0-9.5; per individual average: 5.1, 95%: 2.2-7.9). We used custom Perl
 29 scripts along with a custom C++ program (alleleEst 0.1b) to co-estimate allele frequencies and
 30 genotypes using a Bayesian model (47). Genotype estimates were stored in BIMBAM format as
 31 values ranging from 0 to 2 representing minor allele dosage.

32

33 Following past work (24), we used GENABEL v1.8.0 (48) to perform single locus GWA
 34 mapping analyses. Briefly, we recoded genotype probabilities into genotype values accepted by
 35 GENABEL using a custom Perl script as follows: [0-0.5]=homozygote for major allele, [0.5-
 36 1.5]=heterozygote, [1.5-2]=homozygote for minor allele. Transformed genetic probabilities were
 37 filtered using GENABEL quality control function. SNPs with MAF inferior or equal to 1%, if any,
 38 were excluded from analysis. Individuals with extreme heterozygosity at a false discovery rate
 39 <1% and too high an identity by state (hereafter IBS \geq 0.95, calculated on a subset of 2000
 40 SNPs), if any, were discarded from analysis.

41

42 Analyses were run controlling for population structure using the GENABEL egsscore function
 43 (49). This function extracts principal components of a kinship matrix (here IBS indices)
 44 calculated using a subset of 2000 SNPs. The principal components are then used as covariates in
 45 the GWA linear models. The kinship matrix was computed excluding markers on linkage group
 46 8 (to avoid over-correcting for genome-wide population structure by including causal variants),

1 and excluding markers that were not assigned to linkage groups. We display results in the form
 2 of Manhattan plots. These graphics shows the association score (expressed as $-\log_{10}(pvalue)$) of
 3 every SNP tested along their physical position on the genome. Gaps between scaffolds are not
 4 represented on these graphics. SNP with a significant P-value after Bonferroni correction
 5 (calculated as $0.05/\text{number of tested SNPs}$) are displayed in red in the Manhattan plots.

7 Defining the *Mel-Stripe* locus

9 We combined results from GWA mapping of color and pattern with whole genome
 10 comparative alignments and recombination rate estimates from crosses to define approximate
 11 boundaries for the main locus responsible for color and pattern variation in *T. cristinae* (Figures
 12 S1, S2). We focused on scaffolds 702 and 128 from the melanistic genome, which contained the
 13 overwhelming majority of SNPs significantly associated with color (96%) and pattern
 14 (73%)(numbers refer to significance following a strict Bonferroni correction, i.e., $P < 0.05/(\text{no.}$
 15 of tests)). Our approach included the following steps, which we detail below: (i) generate a
 16 linkage map with the genome scaffolds, (ii) split one key scaffold (702) based on inconsistencies
 17 in the linkage map, (iii) align the green and melanistic morph genomes to each other, (iv) delimit
 18 the *Mel-Stripe* locus based on the total evidence from the mapping results and comparative
 19 alignment. These boundaries are meant to serve as a working hypothesis for the region
 20 controlling color and pattern (which can then be usefully contrasted to the genomic background),
 21 and not as the precise boundaries of the functional variant(s).

22
 23 Linkage map- We used the *LepMap2* software (50) and previously published data from
 24 three F1 crosses to construct a linkage map for the *T. cristinae* melanistic morph genome
 25 sequence scaffolds (the data, comprising 158 million ~ 100 base pair, bp, genotyping-by-
 26 sequencing reads, are fully described in (25)(NCBI BioProject PRJNA356911). Families
 27 consisted of 114 (female melanistic by male green), 48 (female green by male melanistic), and
 28 24 (female green striped by male melanistic) full-sib offspring. However, note that the GWA
 29 described above used a draft (1.3c2) based on only the largest family. Sequence data for the
 30 parents and offspring were aligned to the melanistic morph genome using *bwa aln* and *samse*
 31 (version 0.7.10-r789)(51) with a maximum of 4 miss-matches, and not more than 2 miss-matches
 32 in a 20 bp seed. We then compressed, sorted and indexed the alignments using SAMTOOLS
 33 (1.2)(46), and identified variable nucleotides using the *call* variant caller in BCFTOOLS (version
 34 1.3)(46). We only considered alignments with a mapping quality of 10 or more and bases with a
 35 base quality of 15 or more, and we applied a population prior with theta set to 0.001 when calling
 36 variants and only considered a SNP if the probability of the data assuming the locus was
 37 invariant was less than 0.01. We then applied a variant filter using *vcfutils varFilter* to retain only
 38 those SNPs with a total read depth of 464 and that were more than 5 bp from the nearest gaps
 39 (insertion-deletions).

40
 41 We then generated the genotype input data for the mapping program, *LepMap2*. In doing so,
 42 we used custom Perl scripts to select the subset of SNPs that were recombination informative for
 43 each parent, and then estimated offspring genotype posterior probabilities using the genotype
 44 likelihood from BCFTOOLS (46)(from the *vcf* file) with a prior given by Mendelian inheritance
 45 expectation. We then only retained genotypes when the posterior probability of the most
 46 probable genotype was 0.95 or greater (in other cases the genotype estimate was converted to

1 missing data). From this, we retained 17,478 SNPs (across all three families) for linkage map
2 construction. As a first step with *LepMap2*, we further filtered the data for each family to retain
3 only markers with missing data from fewer than 10 individuals, and with a P-value for
4 segregation distortion greater than 0.005 (i.e., to remove loci with substantial deviations from
5 Mendelian expectations). We allowed for a data error rate of 0.01. This resulted in a total of 4312
6 maternally informative SNPs and 5989 paternally informative SNPs.

7
8 We next used the *LepMap2 SeparateChromosomes* algorithm with a LOD minimum of 4
9 and with a minimum linkage group size of 50 SNPs for initial assignment of SNPs to LGs. This
10 resulted in 6873 SNPs being assigned to 12 linkage groups (i.e., autosomes, *T. cristinae* has 13
11 chromosomes, see below for consideration of the sex chromosome). The *JoinSingles* algorithm
12 was then used to assign additional SNPs to these linkage groups at the lower LOD threshold of 3,
13 if the difference in support between their best and next best possible linkage group differed by 2
14 LOD units. Next we used a custom Perl script and approach to assign entire scaffolds to linkage
15 groups based on the SNP assignments. Specifically, for a scaffold to be assigned to a linkage
16 group (and thus all of its SNPs to be assigned to a linkage groups) required at least two SNPs
17 (and 10% of all SNPs on a scaffold) to have been assigned to that linkage group, and for fewer
18 than half as many SNPs to have been assigned to the next best linkage group. Based on this, we
19 were able to assign 237 scaffolds (which accounted for 89% of all SNPs) to linkage groups.
20 Finally, the *OrderMarkers* algorithm in *LepMap2* was used to estimate marker/SNP order on
21 each linkage group. We took the median position in cM for all markers on a scaffold as the
22 position for each scaffold in each cross.

23
24 As one of the filters applied with *LepMap2* was to remove markers with non-Mendelian
25 patterns of inheritance, we expected to miss the sex (i.e., X) chromosome, and thus to find 12 of
26 the 13 chromosomes, as we did. We thus employed a complementary approach to identify the X-
27 linked scaffolds (in *T. cristinae* males are XO and females are XX)(52). Using SAMTOOLS
28 DEPTH (version 1.2)(51) and custom Perl scripts, we extracted the coverage data from a
29 previously published GBS data set that was used for genome-wide association mapping and
30 comprised 395 female and 197 male *T. cristinae* (data from (24), but aligned to the current
31 genome as described above; we lacked data on offspring sex in the mapping families so used this
32 data instead). We then identified scaffolds where the ratio of read depth for males to females was
33 less than the expected 1:1 ratio expected for autosomal markers (specifically less than 0.75).
34 Twenty-nine scaffolds met this requirement, and also were not assigned to the 12 autosomal
35 scaffolds described above. These included 380 recombination informative markers. Seventeen of
36 these scaffolds were joined into a single linkage group (presumably the X chromosome) using
37 the *SeparateChromosomes* algorithm in *LepMap2* with a LOD limit of 1.5 and a minimum size
38 of 50 SNPs. The 17 scaffolds included 93.4% of the SNPs on the 29 scaffolds we identified as
39 possibly being X-linked based on the coverage ratio. We used *OrderMarkers* to order these
40 markers as described for the X-chromosome.

41
42 *Splitting and re-mapping scaffold 702*- Scaffold 702 from the melanistic morph genome
43 showed a strong association with color and pattern in GWA analyses, but was not originally
44 assigned to a linkage group. Upon examining this further we noted that one large chunk (SNPs
45 up to position 14,171,514) of this scaffold was assigned to linkage group 8 (the linkage group
46 where another scaffold, 128, showed a strong association with color and pattern and where we

1 had previously seen associations with these traits) whereas a second large chunk (SNPs after
 2 position 14,757,049) was assigned to linkage group 5 (preventing placement of this scaffold).
 3 The portion assigned to linkage group 8 showed an association with color and pattern, whereas
 4 the other half of the scaffold did not. Based on this evidence we inferred that this scaffold was
 5 over-assembled and thus we split scaffold 702 into three new scaffolds: 702.1 (positions 1-
 6 14,171,514), 702.2 (starting at position 14,757,049) and 702.3 (the middle ambiguous section
 7 lacking an informative SNP from 14,171,414-14,757,049). The new scaffolds 702.1 and 702.2
 8 were added to their respective linkage groups and the *OrderMarkers* algorithm in *LepMap2* was
 9 re-run for these linkage groups.

10
 11 Whole genome comparative alignment and defining *Mel-Stripe*- We aligned the melanistic
 12 and green morph genomes to each other using *Mugsy* (v1r2.3)(53). Our goal was twofold: (i) to
 13 refine the orientation of scaffolds 702.1 and 128 (the two scaffolds with the greatest association
 14 with color and pattern) based on overlap between these and scaffolds from the green morph
 15 genome, and (ii) to identify possible structural variants associated with the GWA color and
 16 pattern signal. Scaffold 702.1 (from the melanistic genome) partially aligned to green scaffold
 17 1575; green scaffold 1575 also aligned to melanistic scaffold 2963 (which was ‘left’ of scaffold
 18 702.1). Melanistic scaffold 2963 showed a negative correlation between SNP map position and
 19 physical position, suggesting it was in a reverse orientation. This combined with the overlap of
 20 both melanistic scaffolds 2963 and 702.1 with green scaffold 1575 allowed us to also specify
 21 (flip) the orientation of 702.1. Melanistic scaffold 128 was in the correct orientation based on the
 22 correlation (positive) between SNP physical and cM positions. Many small green morph
 23 scaffolds with uncertain orientations span the right side of the re-orientated melanistic scaffold
 24 702.1 and melanistic scaffold 128 (> 15 small scaffolds). No green scaffold was found that
 25 aligned the portion of melanistic scaffold 128 from approximately 5 to 6.4 mbps. This region
 26 also exhibits lower sequence coverage in green individuals, suggesting it might be a large
 27 insertion-deletion polymorphism.

28
 29 Given this information and the GWA mapping signal, we defined the bounds of a putative
 30 *Mel-Stripe* color and pattern locus as comprising melanistic scaffold 702.1 starting from the edge
 31 of the alignment with green scaffold 1575 (702.1 4,139,489 bp) to the edge of 702.1 (bp 1, given
 32 the reverse orientation) along with the neighboring melanistic scaffold 128 from bp 1 to right
 33 edge of the putative insertion-deletion polymorphism (bp 6,414,835). This specific region (that
 34 is, the *Mel-Stripe* locus) contains 70% and 31% of SNPs associated with color and pattern,
 35 respectively (59% of color or pattern-associated SNPs). As a comparison, this region only
 36 contains about 1% of the sequenced SNPs. Thus there is a 61 and 31-fold enrichment of color
 37 and pattern associated SNPs, respectively, in the *Mel-Stripe* locus. As emphasized above, our
 38 main goal was to delimit a *Mel-Stripe* locus that could be contrasted to the genomic background,
 39 and not to precisely identify causal functional variants affecting color and pattern. A schematic
 40 summary of the delimitation of *Mel-Stripe* can be found in Figure S1.

41 42 Genomic change at the *Mel-Stripe* locus

43
 44 We quantified changes at *Mel-Stripe* between time periods using three published data sets:
 45 (1) genotyping-by-sequencing (GBS) data from 1102 individuals collected in a natural
 46 population on *Adenostoma* (FHA) in 2011 and 2013 (n = 500 and 602, respectively)(30, 33), (2)

1 491 re-sequenced whole genomes from an eight-day (i.e., within-generation) release and
 2 recapture field experiment (30), and (3) GBS data from 451 individuals in a between-year (i.e.,
 3 between-generation) field transplant experiment (25). The within-generation experiment
 4 involved releasing 500 *T. cristinae* in a paired-block design and recapturing the survivors (30).
 5 We obtained whole genome sequence data from 491 of these individuals (33), allowing us to
 6 compare allele frequency changes between release and recapture. As described previously (25),
 7 the between-generation experiment involved transplanting 2000 stick insects from a single
 8 variable population (OGA) onto 10 host plant bushes in a block design (five blocks each with
 9 one *Adenostoma* bush and one *Ceanothus* bush per block; 200 *T. cristinae* were released on each
 10 bush). 421 F1 descendants of these individuals were then captured the following year (2011). We
 11 compared 30 individuals representative of the founders (collected in 2010) to the 421 F1s.
 12 Phenotypic change (proportion at time period two minus proportion at time period one) for each
 13 of these three data sets was as follows: FHA, stripe change = 0.06, unstriped change = -0.11,
 14 melanistic change = 0.05; within-generation experiment, stripe change = 0.05, unstriped change
 15 = -0.04, melanistic change = 0.01; between-generation experiment, stripe change = -0.24,
 16 unstriped change = 0.32, melanistic change = -0.07).

17
 18 The GBS data were aligned to the *T. cristinae* reference genome with *bwa* (version 07.10-
 19 r789)(51) using the *aln* and *samse* algorithms. We allowed 5 miss-matches, 2 miss-matches in an
 20 initial 20 bp seed, trimmed bases with phred-scaled quality scores lower than 10, and only placed
 21 reads with a single best match. We then used SAMTOOLS (version 1.2)(46) and the BCFTOOLS
 22 call algorithm (version 1.3)(46) to identify SNPs and calculate genotype likelihoods. We used
 23 the recommended mapping quality adjustment (-C 50), skipped alignments with a mapping
 24 quality less than 20 and bases with a base quality less than 30, and used the multi-allelic SNP
 25 caller with θ set to 0.001 and a posterior probability of 0.01 or less for the homozygous reference
 26 genotype given the data to consider a SNP variable. We then filtered the initial set of SNPs to
 27 retain only those with a mean coverage of $\geq 2X$ (per individual), total coverage (across all
 28 individuals) less than three standard deviations above the mean across all loci, at least 10 reads
 29 of the non-reference allele, a mapping quality of 30, sequence data for at least 80% of the
 30 individuals, a minimum minor allele frequency of 0.01, less than 1% of reads in the reverse
 31 orientation (with our GBS method all reads should be in the same orientation), and separated by
 32 at least 5 bps. Filtering was done using custom Perl scripts. Following filtering, we retained
 33 178,141 SNPs for the natural FHA population and 249,074 SNPs for the between-generation
 34 experiment.

35
 36 We aligned the whole genome re-sequence data from the within-generation experiment to
 37 our reference genome using the *bwa* (version 07.10-r789)(51) mem algorithm with a band width
 38 of 100, a 20 bp seed length and a minimum score for output of 30. We then used SAMTOOLS (46)
 39 to compress, sort and index the alignments, and *Picard Tools* to mark and remove PCR
 40 duplicates (version 2.1.1)(<https://broadinstitute.github.io/picard/>). We then used the *GATK*
 41 HaplotypeCaller and GenotypeGVCFs modules (version 3.7)(54) to call variants and calculate
 42 genotype likelihoods. We used a minimum base quality score of 30 for consideration in
 43 calculations, a prior probability of heterozygosity of 0.001, and called variants with a minimum
 44 phred-scaled confidence of 50. The following filters were then applied using custom Perl scripts:
 45 minimum coverage of 1x per individual, a minimum value of the base quality rank sum test of -
 46 8, a minimum value of the mapping quality rank sum test of -12.5, a minimum value of the read

1 position rank sum test of -8, a minimum ratio of variant confidence to non-reference read depth
 2 of 2, a minimum mapping quality of 40, a maximum phred-scaled P-value of Fisher's exact test
 3 for strand bias of 60, and a minimum minor allele frequency of 0.01. The resulting 6,175,495
 4 SNPs were used for downstream analyses.

5
 6 We obtained maximum likelihood estimates of allele frequencies for all populations /
 7 experimental samples using an expectation-maximization (EM) algorithm, as described in (55).
 8 For this, we used a convergence tolerance of 0.001 and allowed for a maximum of 20 EM
 9 iterations.

10
 11 Population genomic parameters were then calculated based on the *Mel-Stripe* locus and
 12 additional reference loci based on the maximum likelihood allele frequency estimates. Additional
 13 loci were defined for all genome scaffolds placed on linkage groups that contained as many
 14 SNPs as *Mel-Stripe* and were defined by selecting (at random) a contiguous block of SNPs of the
 15 same number as *Mel-Stripe* (FHA: 780 SNPs, 40 reference loci; between-generation experiment:
 16 1180 SNPs, 39 reference loci; within-generation experiment: 47,305 SNPs, 16 reference loci).

17
 18 We analyzed genomic change based on raw allele frequency changes, allele frequency
 19 changes controlling for underlying genetic diversity (i.e., residual change), and using Wright's
 20 Fixation Index (F_{ST}). Specifically, we calculated nucleotide diversity (π) within the 2011 FHA
 21 sample or the founders of each experiment, allele frequency change between these samples and
 22 the 2013 FHA sample (natural FHA population) or recaptured stick insects (both experiments),
 23 the residuals from regressing change on diversity, and $F_{ST} = \frac{\sum(\pi_{total} - \pi_{subpop})}{\sum(\pi_{total})}$. In all cases,
 24 *Mel-Stripe* showed the most extreme change (more than any other locus). Detailed results are as
 25 follows. For FHA, raw change was = 0.0273, residual change was = 0.00516, and F_{ST} was =
 26 0.0051 ($P = 0.024$, Exact probability). For the within-generation experiment, raw change was =
 27 0.0340, residual change was = 0.00212, and F_{ST} was = 0.0030 ($P = 0.059$). For the between-
 28 generation experiment, raw change was = 0.0988, residual change was = 0.0595, and F_{ST} was =
 29 0.0540 ($P = 0.025$; Fisher's combined probability test across data sets: $\chi^2 = 20.50$, d.f. = 6, $P =$
 30 0.0023).

31 Autoregressive-moving-average models fit to different long-term evolutionary data sets

32
 33
 34 We fit Bayesian autoregressive-moving-average (ARMA) models to 10 evolutionary time-
 35 series data sets (details of each data set are given below; two are from *T. cristinae* and the others
 36 from published data in other systems). This approach uses past observations as covariates in a
 37 model. There are two specific types of terms in these models, autoregressive terms (AR) and
 38 moving-average terms (MA). AR terms use the data values from prior years as covariates
 39 whereas the MA terms use residuals from prior years as covariates. Different numbers of prior
 40 years (i.e., different order models) can be considered.

41
 42 Specifics of the models are as follows. We first considered models with order 0, 1 or 2 for
 43 the auto-regressive and moving-average components of the model; a null model with a constant
 44 expectation was included for comparison. As an example, ARMA (1,2) denotes a model with
 45 order 1 for the autoregressive component and order 2 for the moving-average component,
 46 meaning that information from the last year is used for the autoregressive component and that

1 information from the last two years is used for the moving-average component. The general form
 2 of the model is $y_t \sim \text{Normal}(\mu_t, \tau)$ and $\mu_t = c + \sum_i \theta_i y_{(t-i)} + \sum_j \phi_j \varepsilon_{(t-1)}$, where $y_{(t-i)}$ is the data value i
 3 years in the past, $\varepsilon_{(t-1)}$ is the error term from j years, and the sums are over the order of the
 4 autoregressive and moving-average components of the model. We assumed a weakly stationary
 5 model and thus applied the re-parameterization and Beta prior scheme proposed by (56, 57). We
 6 placed a normal prior on the grand mean, $c \sim \text{Normal}(\text{mean} = 0, \text{precision} = 0.01)$, and gamma
 7 prior on the precision for the sampling distribution, $\tau \sim \text{gamma}(0.01, 0.001)$.

8
 9 Each model was fit for each data set and the best model was selected based on deviance
 10 information criterion (DIC; the model with the lowest DIC was chosen). When the null model
 11 was best, the next best model was used for downstream analyses (the null model would not
 12 provide meaningful results for cross-validation or forecasting as the expectation would be the
 13 same for each year). Two estimates of DIC were obtained for each model (to verify consistency),
 14 each based on 10 Markov chain Monte Carlo (MCMC) chains each with 100,000 iterations, a
 15 50,000 step burn-in and a thinning interval of 50. MCMC analyses were conducted using the
 16 *rjags JAGS* interface.

17
 18 We then quantified the predictability of each evolutionary time series using the best ARMA
 19 model. We used two complementary approaches: leave-one-out cross-validation and forecasting.
 20 For leave-one-out cross-validation, we fit the relevant ARMA model for each data set, but with
 21 one year of the data set removed (this was done with each year in turn). The missing year's data
 22 value (evolutionary change) was then predicted from the ARMA model. We used these estimates
 23 to assess the relationship (based on a simple linear model) between the true and predicted
 24 evolutionary change.

25
 26 For forecasting, we dropped the most recent n years of data, where n was (3, 4, ..., 9, 10),
 27 and fit the relevant ARMA model to predict the data values for the dropped data. We then
 28 calculated the Pearson correlation coefficient and coefficient of determination between the
 29 observed and predicted (forecast) change for the dropped years for each value of n . This is
 30 conceptually analogous to predicting/forecasting future (as of yet unobserved) evolutionary
 31 change. Cross-validation and forecasting results were also based on average of results from two
 32 independent MCMC model fits, each comprising 10 chains with 100,000 iterations, a 50,000
 33 iteration burn-in and a thinning interval of 50.

34
 35 The data analyzed include evolutionary time series for discrete trait frequencies, and in the
 36 case of Darwin's finches, quantitative traits (mean value). In both cases, we first obtained point
 37 estimates of the value (mean or frequency) for each generation and then converted these into
 38 evolutionary change data sets (i.e., the data point for year i was the value [mean or frequency] in
 39 year $i+1$ minus the value in year i). The nature and source of each data set are described below.
 40 Results are provided in the main text, Database S1, and Figures S3-S6.

41 42 Long-term field studies in *T. cristinae*

43
 44 We compiled data on morph frequencies in *T. cristinae* using samples collected in the
 45 spring using sweep nets between 1990 and 2017. All individual were scored as 'striped',
 46 'unstriped', or 'melanistic', or occasionally when it was difficult to distinguish between the first

1 two categories as ‘intermediate-striped’. These classifications have been found to be highly
 2 repeatable in past work (26, 35, 36, 58). Samples from 1990 to 1999 were taken and scored by
 3 Cristina Sandoval, who then trained PN in 2000. PN collected and scored most samples from
 4 2000 to 2017.

5
 6 GPS coordinates of all localities were taken at and then used to estimate elevation using
 7 ‘point sampling tool’ on QGIS 2.16.2 (59). The elevation values were extracted from 1/3 arc-sec
 8 Digital Elevation Models (DEM) at the location of the populations’ coordinates. All DEMs were
 9 obtained from United States Geological Survey Dataset (USGS), available at National Map
 10 Viewer (<https://viewer.nationalmap.gov/>). Host-plant collected on (*Ceanothus* or *Adenostoma*)
 11 was recorded for all individuals. We estimated the proportion of individuals in a sample that
 12 were striped (% striped) using all striped and unstriped individuals (excluding melanistic
 13 individuals). We estimated the proportion of individuals in a sample that were melanistic (%
 14 melanistic) using all individuals. Detailed information on these localities (i.e., GPS coordinates
 15 and elevations), morph frequencies, sample sizes, etc. is provided in Database S1.

16
 17 We observed consistent year-to-year increases and then decreases in the frequency of
 18 striped morphs at HV (see main text). We thus computed the binomial probability of the
 19 observed stripe time series alternating between an increase and decrease in stripe frequency
 20 every other year. Specifically, conditional on the first year, we calculated the probability that
 21 every other year showed a reversal in the direction of evolution as $0.5^{17} = 7.6e^{-6}$ (the full time
 22 series includes 18 years, the null probability that evolution reverses direction was assumed to be
 23 0.5, and thus the probability of not changing direction was also 0.5).

24 Climatic data and analyses

25
 26 We collated data on mean springtime statewide temperature in California using publicly
 27 available records (National Centers for Environmental Information,
 28 [https://www.ncdc.noaa.gov/cag/time-series/us/4/0/tavg/3/4/1990-
 29 2016?base_prd=true&firstbaseyear=1901&lastbaseyear=2000](https://www.ncdc.noaa.gov/cag/time-series/us/4/0/tavg/3/4/1990-2016?base_prd=true&firstbaseyear=1901&lastbaseyear=2000)). We focused on temperature
 30 averages across March, April, and May as these are the three months that *T. cristinae* is by far
 31 most active (most of the rest of the year is spent in egg diapause)(26, 34, 58). Nonetheless, we
 32 present results from different combinations of spring months below.

33
 34
 35 We fit a hierarchical Bayesian model for the full *T. cristinae* color data set, using data from
 36 all populations (i.e., not just HV) collected from 1990 to 2017. We did so to: (i) test for an
 37 association between climate and the melanistic morph frequency, and (ii) determine how well
 38 climate predicts color morph frequency across space and time.

39
 40 We assumed a binomial sampling distribution for the observed number of melanistic
 41 morphs for a site and year (y_{ij}) given the number of *T. cristinae* sampled (n_{ij}) and the true
 42 melanistic morph frequency (p_{ij}). We connected this to a linear model with the logit link
 43 function, such that $\text{logit}(p_{ij}) = \alpha_i + \beta_i x_{\text{temperature}} + \theta x_{\text{year}} + \varepsilon_{ij}$, where α_i is a population (site)
 44 specific intercept, β_i denotes the effect of climate (temperature, see details below) on melanistic
 45 morph frequency for population i , θ is an overall effect of year (allowing for a general increase
 46 or decrease in melanistic morph frequency), and ε_{ij} is an error term that accounts for over-

1 dispersion relative to binomial sampling. We gave the ϵ values a normal prior with mean of 0 and
 2 precision parameter $\tau \sim \text{gamma}(0.1, 0.01)$ (we imposed a sum-to-zero constraint on the ϵ values).
 3 We then defined linear models at the next level of the hierarchy for the population specific α and
 4 β coefficients (for the intercept and effect of temperature, respectively), such that,

$$5 \quad \alpha_i = a_1 + b_1 x_{\text{elevation}} + c_1 x_{\text{host}} + d_1 x_{\text{mountain}}$$

$$6 \quad \beta_i = a_2 + b_2 x_{\text{elevation}} + c_2 x_{\text{host}} + d_2 x_{\text{mountain}}$$

7
 8 Here, $x_{\text{elevation}}$ is the elevation at a location, x_{host} is a binary indicator variable for host plant
 9 (*Adenostoma* = 0, *Ceanothus* = 1), x_{mountain} is a binary indicator variable denoting the mountain
 10 range (0 = Highway 154; 1 = Refugio), and $a_1, a_2, b_1, b_2, c_1, c_2, d_1$ and d_2 are regression
 11 coefficients (all given Normal priors with mean 0 and precision 0.0001).
 12
 13
 14

15 We fit this model with three different temperature variables: (i) mean temperature for
 16 March, April and May (when *T. cristinae* are most active), (ii) mean temperature for February,
 17 March, April and May, and (iii) mean temperature for February, March and April. We used the
 18 *rjags* interface with JAGS to obtain Markov chain Monte Carlo (MCMC) parameter estimates
 19 for the model parameters. In each case, we ran three chains, each with a 10,000 iteration burn-in,
 20 25,000 post burn-in iterations and a thinning interval of 10. We used four-fold cross-validation to
 21 determine the predictive power of the models. Specifically, we split the data set into four random
 22 subsets (only considering cases where the sample size was 25 or greater) and used three subsets
 23 to fit the model and validated the model by predicting morph frequencies for the other subset
 24 (MCMC options identical to those for the main models were used).
 25

26 Temperature was generally associated with a higher frequency of melanistic *T. cristinae* (a_2
 27 was positive), but less so at *Ceanothus* sites (c_2 was negative) (Table S2; estimates of the effect
 28 of temperature for each site and year are shown in the main text). Melanistic morphs were less
 29 common at higher elevations and on Refugio independent of temperature. Cross-validation
 30 results showed that the models had significant but modest predictive power. For example, with
 31 the March, April, May temperature model, the Pearson correlation between observed and
 32 predicted melanistic morph frequencies was $r = 0.16$ (95% CIs = 0.040-0.28, $P = 0.0102$, r^2 from
 33 a linear model = 0.027). The other temperature variables gave similar results: February, March,
 34 April, May temperature, $r = 0.15$ (95% CIs = 0.025-0.27, $P = 0.0188$, r^2 from a linear model =
 35 0.022); February, March, April temperature, $r = 0.19$ (95% CIs = 0.069-0.31, $P = 0.0024$, r^2 from
 36 a linear model = 0.037).
 37

38 Thermoregulatory experiments

39
 40 We conducted lab thermoregulatory experiments testing the desiccation / heat tolerance of
 41 green versus melanistic *T. cristinae*. Heat stemmed from a desk lamp (K-mart model ksn: 0-
 42 02546202-9), raised 4.5 inches above two petri dishes that were stacked on top of each other and
 43 pushed to touch the base of the lamp. A third petri dish containing an individual *T. cristinae* was
 44 placed on top of the other two. The bulb used a Sylvania A19 halogen 100-watt replacement that
 45 used 72-watts. A total of four such lamp set-ups were used, allowing simultaneous assays of four
 46 *T. cristinae* (always two green and two melanistic, assigned randomly to one of the four lamps at

1 the initiation of an assay, and then randomly re-assigned to one of the four after each weighing
 2 census, see below). Details of the procedure were as follows. Each individual was weighed. Each
 3 lamp was then turned on for ten minutes. Placing test animals underneath the lamps then started
 4 the trials. Every twenty minutes all four individuals were removed simultaneously and weighed
 5 in a random order, and scored as dead or alive. They were then assigned randomly back to one of
 6 the four test lamps. This procedure was repeated until 180 minutes had passed. A total of eight
 7 sets of such trials were run (total $n = 32$).

8
 9 We fit a Cox proportional hazards model to the survival data to test for an effect of morph
 10 (green versus melanistic) on survival (60). For this, we used the *survival* package in R (61). We
 11 used the exact partial likelihood method, which is advantageous relative to the more common
 12 Efron method when time is measured in discrete intervals and tied times of death are thus more
 13 likely. We detected a significant effect of morph on survival time ($\exp(B) = 3.57$, 95% CIs =
 14 1.34-9.51, $P = 0.0111$). Note that $\exp(B) > 1$ indicates melanistic morphs died from desiccation
 15 more rapidly than green morphs.

16 Estimating genotype-specific fitness using genomic data

17
 18
 19 We estimated selection coefficients/relative fitnesses for different genotypes at the *Mel-*
 20 *Stripe* locus based on the within-generation release-recapture experiment and based on patterns
 21 of evolutionary change between the 2013 and 2011 FHA samples. Similar to (23) we used PCA
 22 and k-means clustering to assign individuals one of six *Mel-Stripe* genotypes: homozygous for
 23 the stripe haplotype/allele (s/s), homozygous for the green unstriped haplotype (u/u),
 24 homozygous for the melanistic haplotype (m/m), or one of the three possible heterozygotes (s/u ,
 25 s/m or u/m) (Fig. S2). We conducted a PCA on the individual genotype matrix for each of the two
 26 data sets. This was done for all individuals and the 780 SNPs comprising the *Mel-Stripe* locus.
 27 We then clustered *T. cristinae* based on the first two genetic PCs with k-means clustering; this
 28 was done with the R *kmeans* function with six centers, 100 starts and a maximum of 200
 29 iterations. An initial round of clustering was performed to define cluster centers. For this round
 30 an equal number of green, striped and melanistic individuals were used (42 of each, which was
 31 the number of green individuals). We then used those centers to cluster all individuals with a
 32 second round of k-means clustering (this included individuals with no phenotypic data).
 33 Assignments from k-means clustering corresponded well with groups of individuals with the
 34 same color/pattern (i.e., stripe) phenotype, and were the basis for designating genotypes.

35
 36 For the within-generation experimental data, we fit a Bayesian beta-binomial model to infer
 37 fitness values. Here, we inferred the survival probability of individuals with each genotype using
 38 a binomial sampling distribution for the number of recaptures given the probability of survival
 39 and recapture (p_{genotype}) and the number of individuals released with that genotype (n_{genotype}). We
 40 assigned an uninformative (Jeffery's) beta prior for each survival probability. Posterior samples
 41 ($N = 5000$ each) were obtained from the closed form solution for the posterior using *R* (62), and
 42 were then used to calculate the relative fitness of each genotype by dividing the survival
 43 probability by the survival probability with the highest fitness (based on the point estimate; s/s).

44
 45 An alternative model was required for the FHA data, which was based on change over two
 46 generations (2011 versus 2013). During this time haplotype frequencies went from $m = 0.316$, s

1 = 0.602, and $u = 0.082$ to $m = 0.360$, $s = 0.570$, and $u = 0.071$. Perhaps more importantly, in both
 2 years, we detected an excess of the s/m heterozygotes (0.514 in 2011 and 0.502 in 2013) relative
 3 to Hardy-Weinberg expectations (0.380 and 0.410, respectively). For this analysis, we assumed
 4 the following relative fitness values: $s/m = 1$ (based on observed patterns of change this genotype
 5 appeared to have the highest fitness), $m/m = 1 + s1$, $s/s = 1 + s2$, $u/u = 1 + s2 + s3$, $s/u = 1 + s2 +$
 6 $s3 * s4$, and $m/u = 1 + s1 + s3 * s4$. Thus, $s1$ and $s2$ define the fitness value of the m/m and s/s
 7 homozygote in a way that allows for any form of dominance. In turn, $s3$ defines the fitness of u/u
 8 relative to s/s (i.e., after adding $s2$). The s/u heterozygote is $1 + s2 + s3 * s4$, thus $s4$ is the
 9 heterozygous effect. This is similar for m/u . We took an approximate Bayesian computation
 10 (ABC) approach to estimating the selection coefficients. We first sampled selection coefficients
 11 from their priors, $U(-0.5, 0.5)$ for $s1$, $s2$, and $s3$, and $U(0,1)$ for $s4$. We then simulated evolution
 12 forward in time for two generations according to a Wright-Fisher model with the observed
 13 starting genotype frequencies, and dynamics governed by drift and the sampled the selection
 14 coefficients (assuming viability selection). We assumed a variance effective population size of
 15 110.3, which was inferred from patterns of change across 178,141 SNPs (following general
 16 procedures outlined in (63)). We ran 1,000,000 ABC simulations. We then used the ridge
 17 regression adjustment method in the R *abc* package to obtain samples from the posterior
 18 distribution from the simulation output. We retained the top 0.5% of simulations with the
 19 smallest distance between the simulated and observed genotype frequencies in the 2013 sample.
 20 We then converted the estimates of selection coefficients to relative fitnesses.

21

22 Field experiment testing for NFDS

23

24 We implemented a field transplant experiment testing for NFDS. A total of 1000 individuals
 25 were transplanted, collected from March 21-24, 2017 from populations PRNC (latitude 34.53,
 26 longitude -119.85), OUTA (latitude 34.53, longitude -119.84), HVC (latitude 34.49, longitude -
 27 119.79), and HVA (latitude 34.49, longitude -119.79). Numbers were as follows: green-unstriped
 28 morphs, PRCN 220, OUTA 50, HVC 140, HVA 90; green-striped morphs, PRCN 30, OUTA
 29 100, HVA 280, HVC 90. Individuals were kept in groups of 10 and each group was randomly
 30 assigned to one of two treatments: striped individuals common (40 striped and 10 unstriped
 31 individuals) versus striped individuals rare (10 striped and 40 unstriped individuals). Each of
 32 these groups of 50 individuals was then randomly assigned to one of 20 experimental bushes (in
 33 the general area of latitude 34.51 and longitude 119.80). Each bush was cleared of existing *T.*
 34 *cristinae* (the only *Timema* species occurring in this area) by sampling it each day March 21-24.
 35 Past work demonstrates that this clears bushes of the overwhelming majority of *Timema* (25, 26,
 36 58). Nonetheless, as an additional measure for ensuring accurate identification of experimental
 37 animals, each transplanted individual was marked with fine tip sharpie on the underbelly. This
 38 mark allowed us to distinguish experimental animals from any remaining residents, and the
 39 marks are not visible when *Timema* are resting on leaves. Individuals were released on March
 40 26th between 9am and 3pm. Each individual was released with tweezers onto an experimental
 41 plant and checked to cling well to their transplanted host. Individuals were recaptured using
 42 visual surveys and sweep nets on March 31st, as in past work (25, 26, 30, 35, 36, 58), and scored
 43 as striped or unstriped.

44

45 We fit a Bayesian beta-binomial model to assess the effect of initial stripe frequency on the
 46 recapture stripe frequency. We assumed that the recapture stripe count for bush i was $y_i \sim$

1 binomial(p_i, n_i), where p_i is the true stripe recapture rate for a given initial release stripe
 2 frequency. We then placed independent, uninformative beta priors on p_i for each treatment.
 3 MCMC (via *rjags*) was then used to draw samples from posterior distribution. Stripe frequencies
 4 clearly increased when stripe was initially rare (recapture frequency = 0.46, 95% CIs = 0.37-0.55;
 5 change in stripe frequency = 0.26, 95% CIs = 0.17-0.35; posterior probability that stripe
 6 increased > 0.99). In contrast, we found no clear, consistent pattern of change when stripe was
 7 initially common (change in stripe frequency = -0.006, 95% CIs = -0.093-0.063; posterior
 8 probability that stripe increased > 0.43). We inferred selection coefficients for each treatment
 9 (20% vs. 80% initial stripe frequency) based on the estimated posterior distribution for the true
 10 stripe recapture rate. We defined relative fitnesses for striped and green stick insects as $w_{stripe} = 1$
 11 and $w_{green} = 1 - s$, respectively. Here s is the selection coefficient. We then estimated w_{green} based
 12 on the difference between release and recapture frequencies of the striped morph, such that $p_i =$
 13 $(p_0 w_{stripe}) / (p_0 * w_{stripe} + (1-p_0) * w_{green})$, which can be rearranged as $w_{green} = (p_0 * p_i - p_0) / ((p_0 - 1) *$
 14 $p_i)$. Here p_0 is the stripe release frequency (0.2 or 0.8).

15

16 Estimation of differences between hosts

17

18 We fit a hierarchical Bayesian model to quantify the overall difference in stripe frequency
 19 between hosts across years. A key aspect of this model was that it allowed us to account for the
 20 heterogeneity in sampling, including the fact that a subset of sites was sampled each year. We
 21 used all samples from the main mountain, Highway 154. This included 21,067 data points (*T.*
 22 *cristinae* scored as striped versus unstriped, we excluded melanistic morphs) from 274
 23 collections (site by year combinations; 29 sites with a mean of 9.4 visits per site) spanning 27
 24 years (1990 to 2017).

25

26 We specified generalized linear models for the stripe frequency at each location (site) for
 27 each year (nearby or inter-digitated samples from different hosts were considered different sites).
 28 We included effects for site and year, and modeled each of these hierarchically by placing a
 29 normal prior on them with parameter values estimated from the data (except the means for the
 30 year effects, which were fixed at 0 to ensure the model parameters were identifiable). We placed
 31 uninformative priors on the site means, normal with mean 0 and precision $1e^{-6}$, and on the
 32 precision parameters, gamma(0.01, 0.001). We used Markov chain Monte Carlo to generate
 33 samples from the posterior distribution and used these samples to compute several key derived
 34 parameters: the yearly mean stripe frequency for each host and the yearly mean difference in
 35 stripe frequency between hosts. Inferences were based on three MCMC chains, each with a
 36 10,000 iteration burn-in, 20,000 sampling iterations and a thinning interval of 5 (MCMC
 37 analyses were conducted with *rjags*). Point estimates (posterior medians) for the difference
 38 between hosts (stripe frequency on *Adenostoma* minus *Ceanothus*) ranged from 0.30 to 0.64
 39 (mean = 0.56), and for all but one year (2011) the 95% CIs for the difference in stripe frequency
 40 excluded 0 (i.e., they were significantly positive).

41

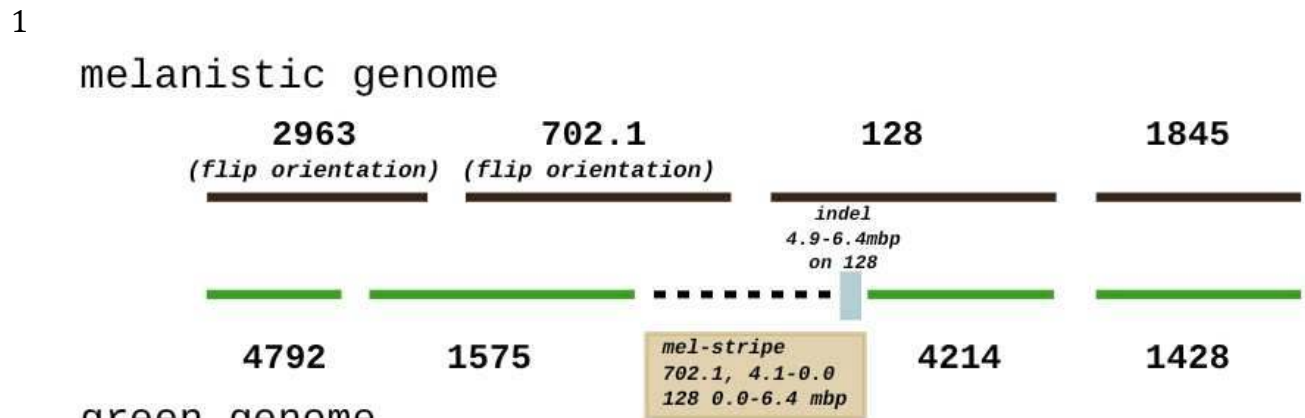
42 Estimating predictability in finches and moths

43

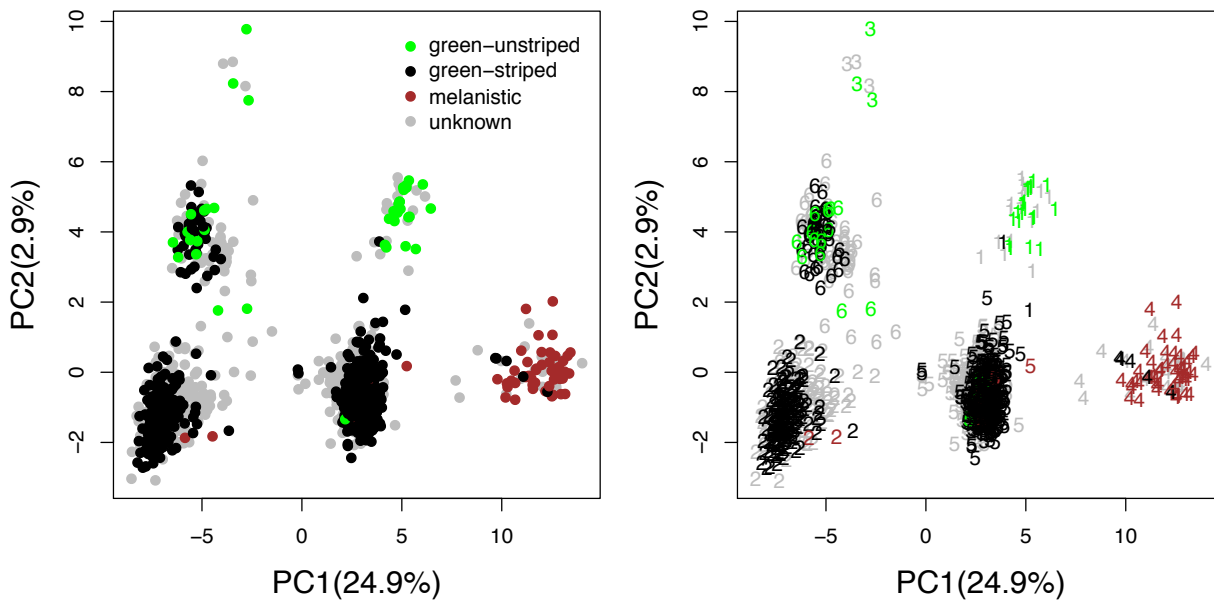
44 The data analyzed were obtained as follows. We obtained data on *Geospiza fortis* and
 45 *Geospiza scandens* body size and beak size from (21). The data are from Daphne Major from
 46 1973 to 2012. Three measurements were included: principal components (PC) 1 body size, PC1

1 beak size and PC2 beak size. We obtained data on *Panaxia dominula medionigra* allele
2 frequency from (40). We used the data from 1940-1978, as there were no gaps in sampling
3 during this time interval. We obtained data on *Biston betularia* peppered moth morph frequency
4 from (41). We used the data from Leeds, which was most complete, and restricted analysis to
5 years 1967 to 1995 because there were several years after 1995 with very low sample sizes.
6 ARMA Models were fit to the data as described for *T. cristinae* above.
7

8 We then asked whether and to what extent including rainfall data on Daphne Major (also
9 from 1973 to 2012) improved the fit of the *Geospiza* time series data sets. We focused on rainfall
10 as it is thought to be a strong determinant of seed size, which is a key source of selection on
11 these finches (1, 21). We obtained the rainfall data from (21). We fit Bayesian ARMA models of
12 order 0, 1, or 2 with respect to the AR and MA components (as described previously) that also
13 included rainfall (MCMC details were identical to those described above). We placed an
14 uninformative prior, Normal(mean = 0, precision = 1e-5), on the coefficient for rainfall. We then
15 used the best ARMA model that included rainfall (based on DIC) for predictive cross-validation
16 and forecasting as described above for the pure ARMA models (without rainfall). We then
17 compared the predictive performance of the best ARMA models with and without rainfall.

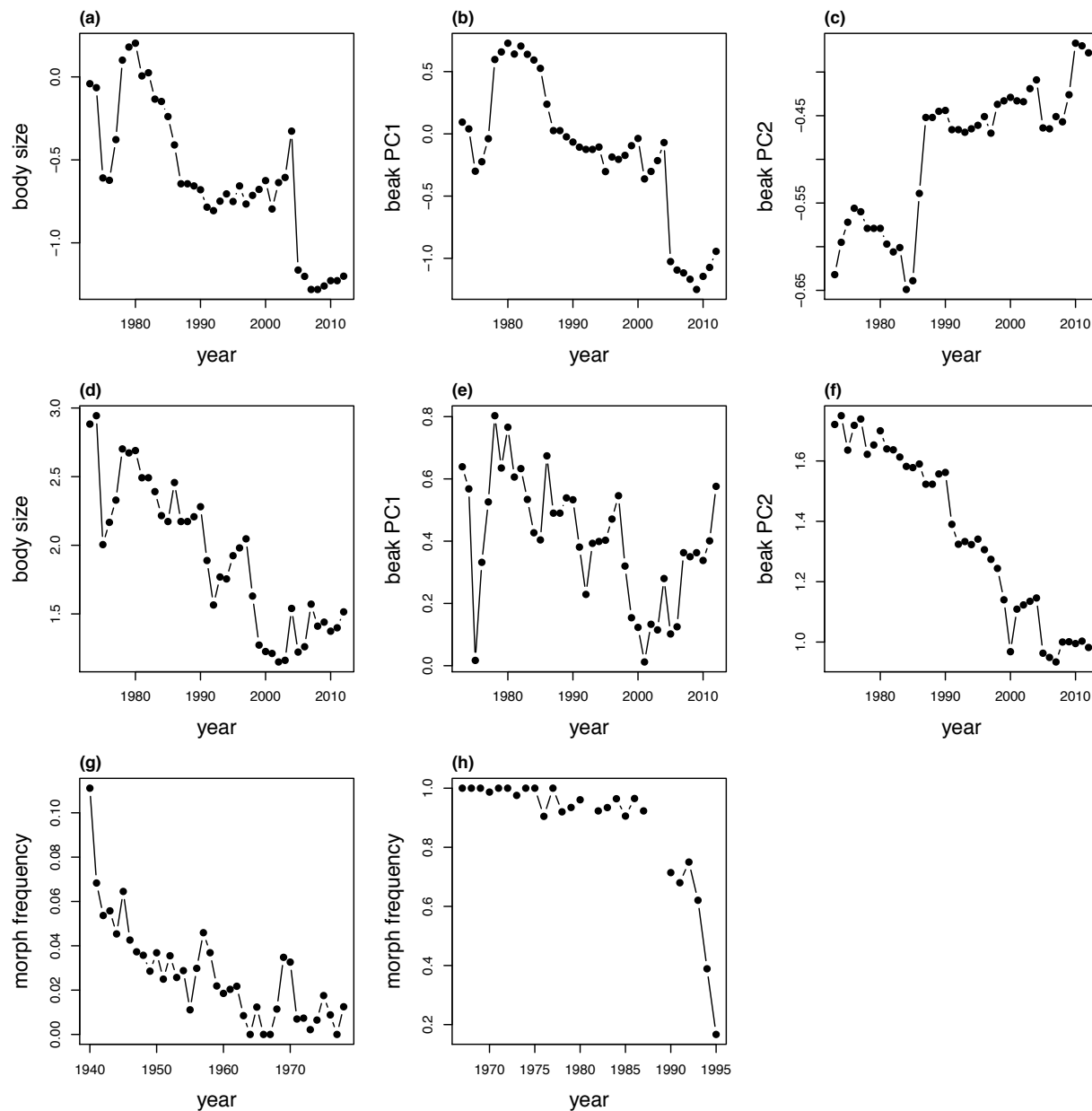


3 **Fig. S1. Schematic illustrating the delimitation of the Mel-Stripe locus using two reference**
 4 **genomes. See text of supplementary materials for details.**
 5

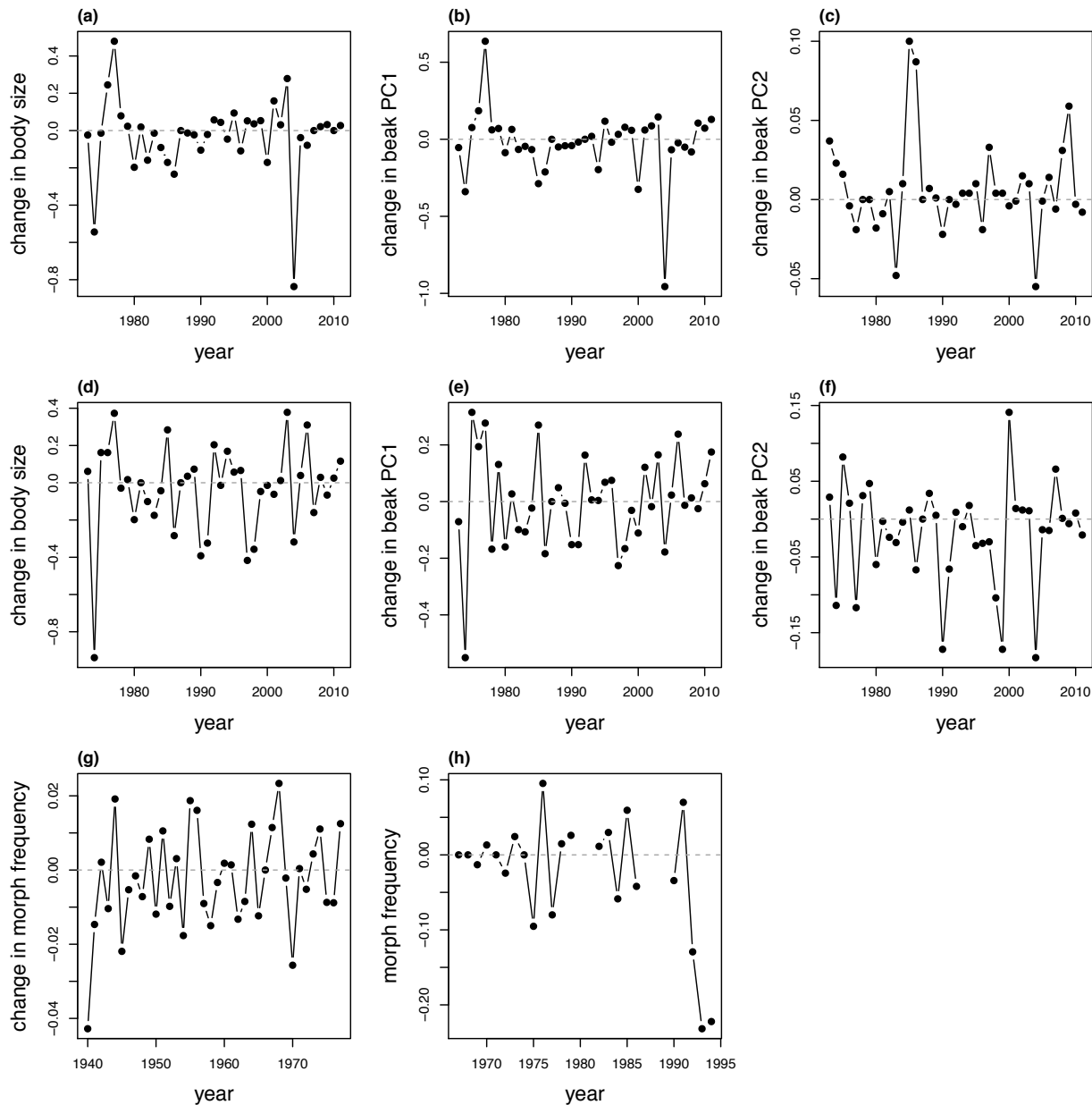


1
 2 **Fig. S2. Principal Components Analysis (PCA) ordination of 1102 *T. cristinae* from FHA**
 3 **based on genetic data from the Mel-Stripe locus. Points (left panel) and numbers (right**
 4 **panel) denote individuals, and are colored based on color and pattern phenotypes (we did**
 5 **not have phenotypic data for some individuals). In the right panel, numbers denote**
 6 **cluster/group assignments from k-means clustering with k=6. Cluster assignments were**
 7 **used to assign genotypes when estimating selection.**

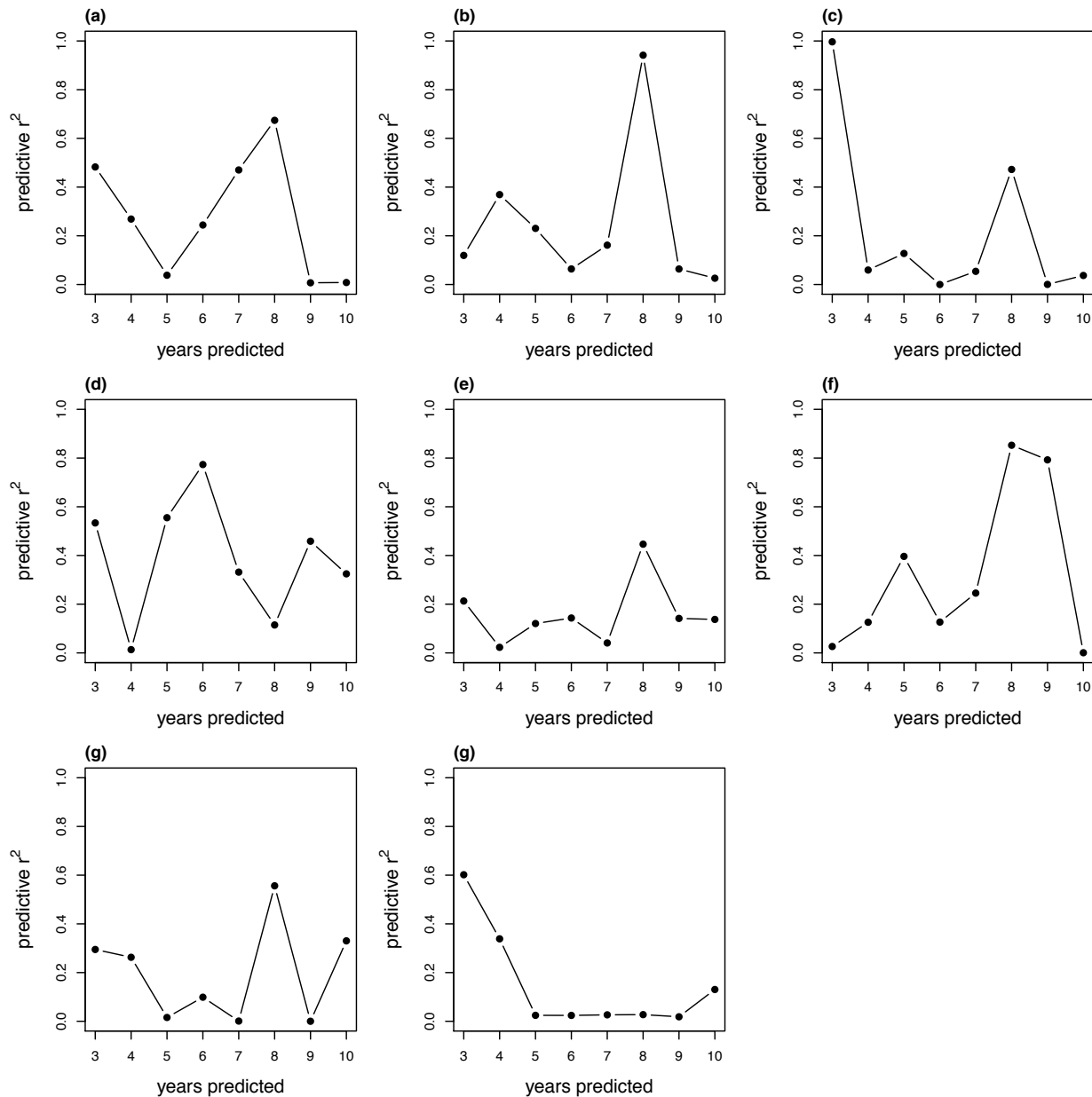
8
 9



1
 2 **Fig. S3. Evolutionary time series for *Geospiza fortis* body size (a), beak PC1 (b), beak PC2**
 3 **(c), *G. scandens* body size (d), beak PC1 (e), beak PC2 (f), *Panaxia dominula medionigra***
 4 **frequency (g), and *Biston betularia* "peppered" frequency.**
 5

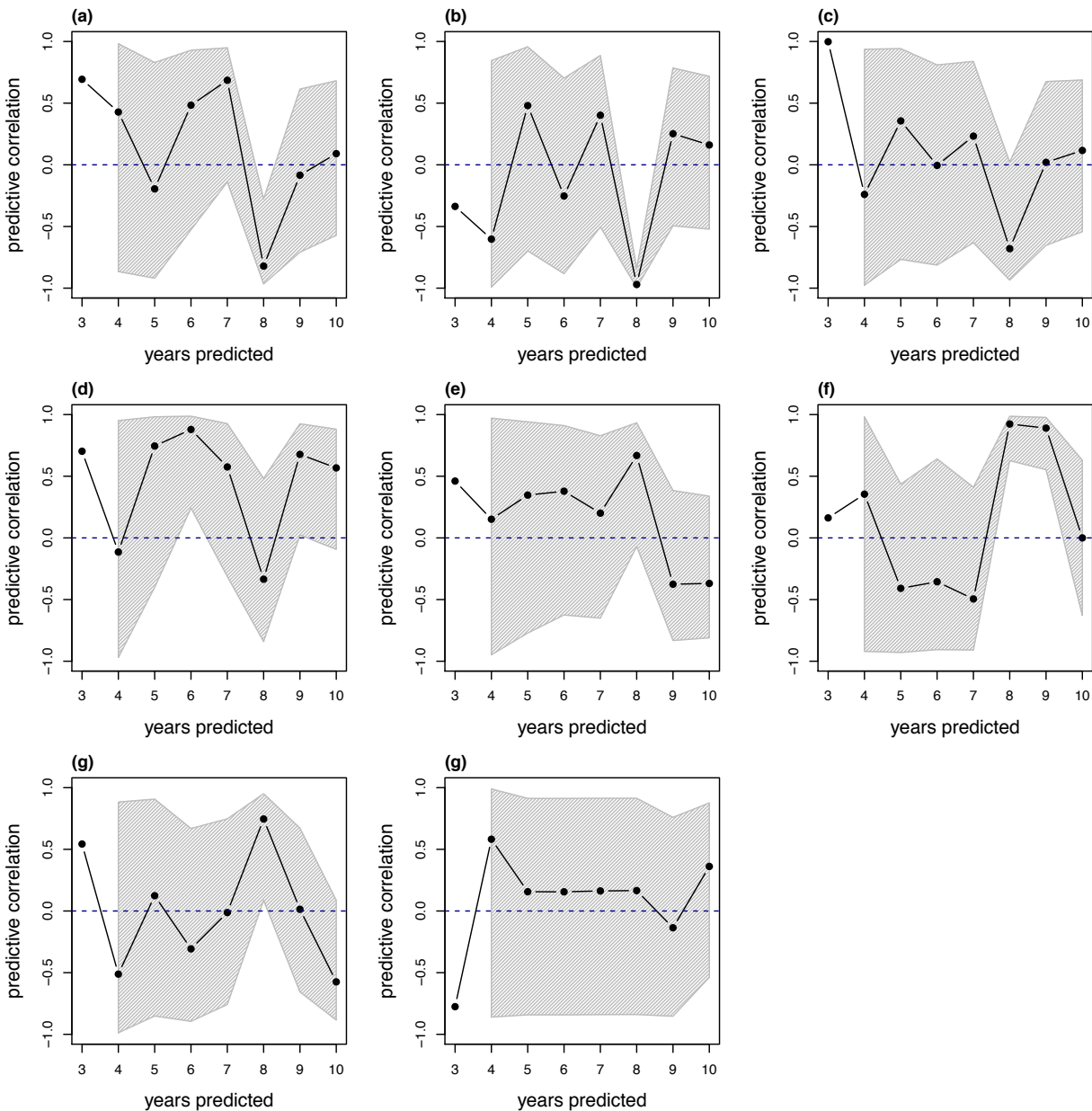


1
 2 **Fig. S4. Change in mean trait values or morph/allele frequency for *Geospiza fortis* body size**
 3 **(a), beak PC1 (b), beak PC2 (c), *G. scandens* body size (d), beak PC1 (e), beak PC2 (f),**
 4 ***Panaxia dominula medionigra* frequency (g), and *Biston betularia* "peppered" frequency.**
 5 **Data points for each year denote that change observed from that year to the next year.**
 6
 7



1
 2 **Fig. S5. Predictive r^2 from ARMA forecasting models for evolutionary time series in**
 3 ***Geospiza fortis* body size (a), beak PC1 (b), beak PC2 (c), *G. scandens* body size (d),**
 4 **beak PC1 (e), beak PC2 (f), *Panaxia dominula medionigra* frequency (g), and *Biston betularia***
 5 **"peppered" frequency. r^2 between the observed and predicted values of change are shown**
 6 **from models dropping (and predicting) the last three to 10 years (r^2 was computed from a**
 7 **simple linear model).**

8



1
 2 **Fig. S6. Predictive correlations from ARMA forecasting models for evolutionary time**
 3 **series in *Geospiza fortis* body size (a), beak PC1 (b), beak PC2 (c), *G. scandens* body size (d),**
 4 **beak PC1 (e), beak PC2 (f), *Panaxia dominula medionigra* frequency (g), and *Biston***
 5 ***betularia* "peppered" frequency. Pearson correlations (solid line and points) and 95%**
 6 **confidence intervals (shaded polygons) between the observed and predicted values of**
 7 **change are shown from models dropping (and predicting) the last three to 10 years.**

8

1 **Table S1. Summary of cross-validation and forecasting results (values for forecasting are**
 2 **medians from estimates based on 3 to 10 year forecasts). Bold font denotes cases where the**
 3 **ARMA model was preferred over a null model with a constant expectation.**

Data set	Best model	cross-validation intercept	cross-validation slope	cross-validation r^2	forecasting r	forecasting r^2
<i>Timema</i> stripe	ARMA(1,2)	-0.005463	0.938310	0.6974	0.9282905	0.8618326
<i>Timema</i> color	ARMA(1,2)	0.03373	-1.24295	0.1019	-0.2959806	0.1388707
<i>G. fortis</i> body size	ARMA(2,2)	-0.07142	-1.89589	0.2581	0.2593157	0.2565920
<i>G. fortis</i> beak size (PC1)	ARMA(0,1)	-0.1872	-6.0475	0.2769	-0.0460291	0.1405218
<i>G. fortis</i> beak size (PC2)	ARMA(0,1)	0.002860	0.462132	0.03286	0.06829066	0.05675793
<i>G. scandens</i> body size	ARMA(1,2)	-0.005377	-0.159569	0.05488	0.6263869	0.3951535
<i>G. scandens</i> beak size (PC1)	ARMA(1,2)	0.02175	-0.22193	0.05206	0.2741161	0.1395220
<i>G. scandens</i> beak size (PC2)	ARMA(1,2)	-0.002938	0.546308	0.05978	0.08118622	0.18602100
<i>P. dominula</i> medionigra	ARMA(1,1)	-0.0005844	0.4419179	0.01698	0.000594893	0.180800958
<i>B. betularia</i> peppered	ARMA(1,0)	-0.05174	-1.80925	0.6584	0.15945025	0.02692756

4
5

1 **Table S2. Posterior median and 95% credible intervals for key model parameters from the**
 2 **March, April, May melanistic morph model. All continuous covariates were standardized.**

Parameter	Median	Lower bound 95% CI	Upper bound 95% CI
a_1	-2.31	-2.44	-2.20
a_2	0.187	0.063	0.309
b_1	-0.163	-0.260	-0.061
b_2	-0.0060	-0.0151	0.0274
c_1	0.164	-0.001	0.341
c_2	-0.197	-0.362	-0.249
d_1	-0.500	-0.749	-0.249
d_2	-0.050	-0.323	0.219

3
4

1 **Table S3. Summary of model fit for the *Geospiza* data when rainfall is included in the**
 2 **model (based on rainfall and trait measurements from 1973-2012). We report the r^2 (mean**
 3 **across 3-10 years) for forecasting for the best ARMA model with rainfall, as well as the**
 4 **change in forecasting r^2 , r (unsquared), and the lower and upper bounds on of the 95%**
 5 **confidence interval on r (lb and ub, respectively)(all of these values are averages across 3-**
 6 **10 year forecasts) obtained by including rainfall (positive values mean that rainfall**
 7 **improved the predictive forecast).**

Data_set	Model	r^2	Change in r^2	Change in r	lb	ub
<i>G. fortis</i>						
body size	ARMA(2,2)	0.434	0.178	0.238	0.192	0.102
beak PC1	ARMA(0,1)	0.174	0.034	0.365	0.027	0.116
beak PC2	ARMA(0,1)	0.080	0.023	0.207	0.078	0.047
<i>G. scandens</i>						
body size	ARMA(2,1)	0.059	-0.337	-0.632	-0.421	-0.206
beak PC1	ARMA(1,2)	0.249	0.109	-0.476	0.014	-0.210
beak PC2	ARMA(1,2)	0.121	-0.065	-0.054	0.002	0.100

8

9

1 Database S1. Raw population data. See attached .csv sheet. Variable names are as follows:
2 location = population/locality, year = year collected, latitude = latitude, longitude =
3 longitude, elevation = elevation in meters, host = host plant collected on (A = *Adenostoma*,
4 C = *Ceanothus*), melanistic = number of melanistic individuals collected, striped = number
5 of striped individuals collected, unstriped = number of unstriped individuals collected,
6 intermediate = number of intermediately striped individuals collected, total = total number
7 of individuals collected, proportion_melanistic = proportion of the sample that was
8 melanistic, proportion_striped_no_mel = proportion of the sample that was striped
9 (excluding melanistics), mean_FebMarApr_temp = mean temperature in Fahrenheit for
10 February, March, and April, mean_MarAprMay_temp = mean temperature in Fahrenheit
11 for March, April, and May, mean_FebMarAprMay_temp = mean temperature in
12 Fahrenheit for February, March, April, and May, refugio_yn = Mountain collected on (1 =
13 Refugio, 0 = Highway 154).

14

15

16

17

18

19

20

21

The three morphs of *Timema cristinae*

Unstriped



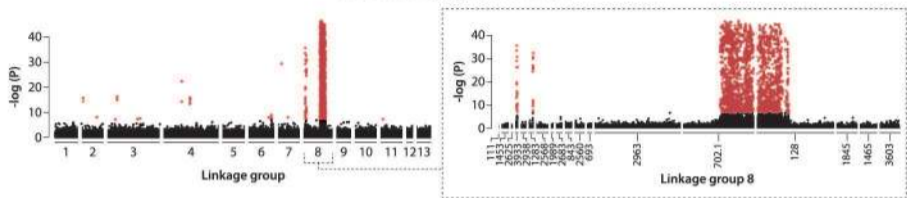
Striped



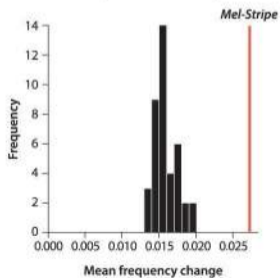
Melanistic



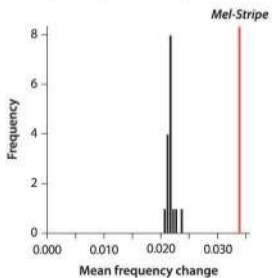
A. GWAS mapping of color variation



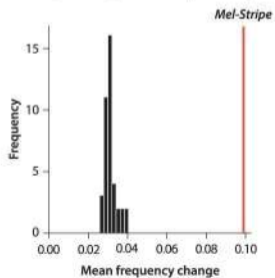
B. Allele frequency change through time (FHA 2011 vs. 2013)



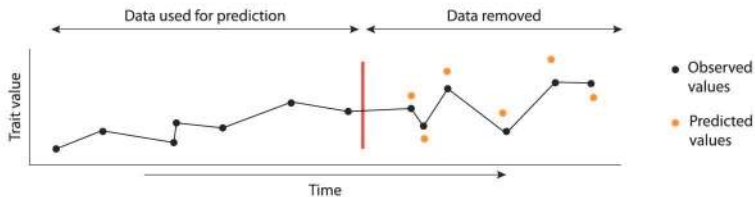
C. Allele frequency change through time (within-generation experiment)



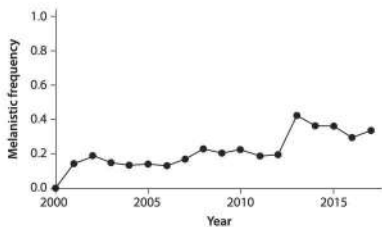
D. Allele frequency change through time (between-generation experiment)



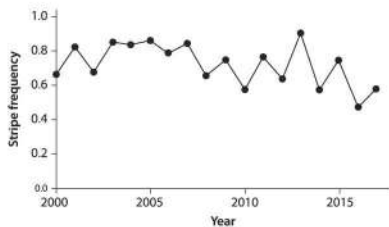
A. Predicting evolution via multi-year forecasting



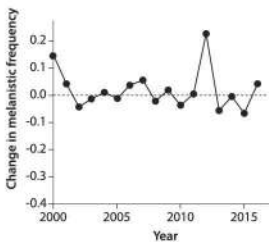
B. Color morph frequencies through time



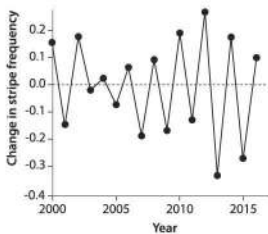
C. Pattern morph frequencies through time



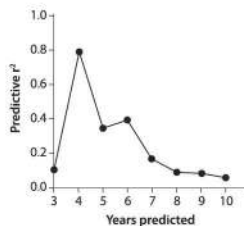
D. Change in color morph frequencies



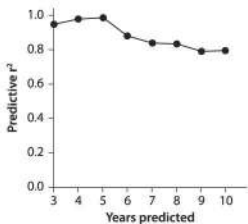
E. Change in pattern morph frequencies



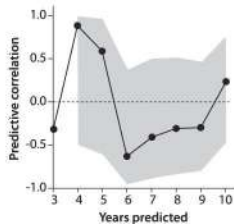
F. Predicting change in color morph frequencies (r^2)



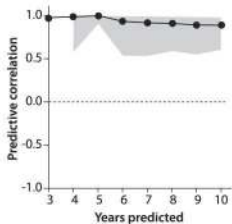
G. Predicting change in pattern morph frequencies (r^2)



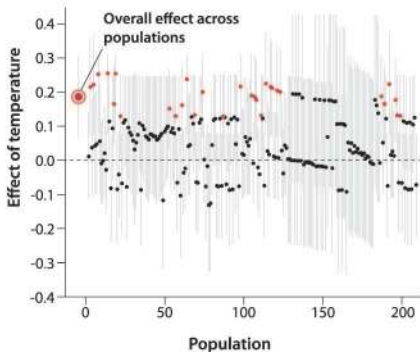
H. Predicting change in color morph frequencies (r)



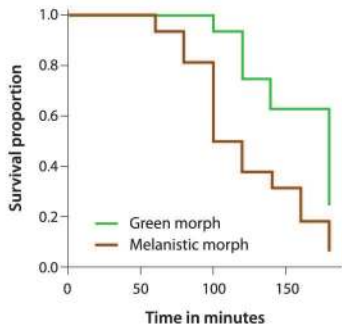
I. Predicting change in pattern morph frequencies (r)



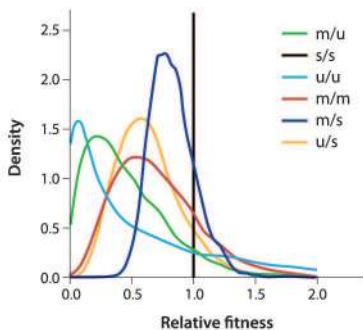
A. Yearly temperature and melanistic frequencies



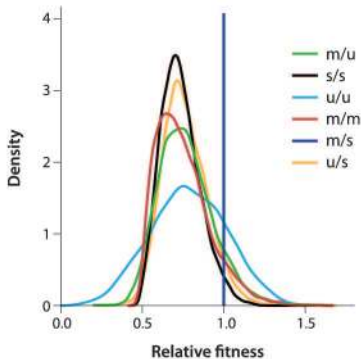
B. Heat tolerance in lab experiments



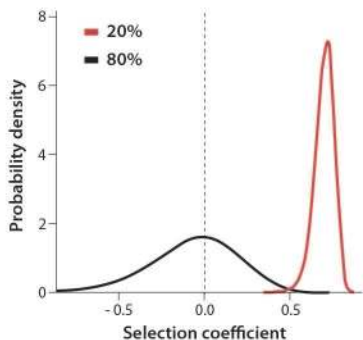
C. Selection in the within-generation experiment



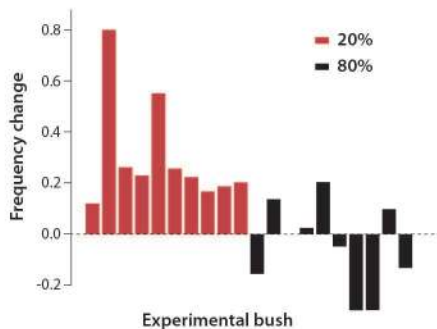
D. Selection in FHA between 2011 and 2013



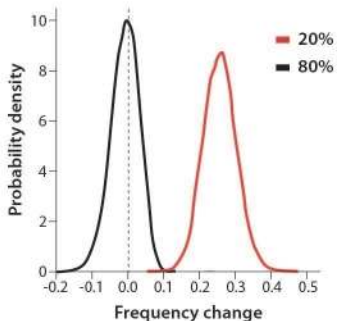
A. Posterior probability of selection coefficient per treatment



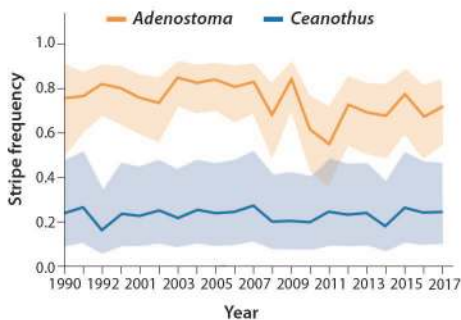
B. Frequency change (% stripe recaptured minus % striped released) on each experimental bush



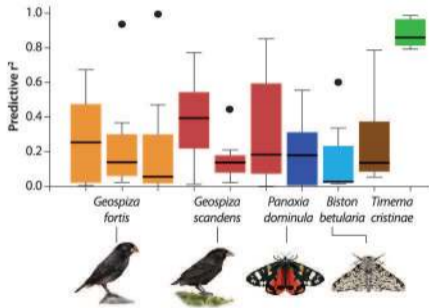
C. Posterior probability of frequency change per treatment



D. Striped morph frequency across the 25-year study period



A. Predicting evolution in studies (r^2)



B. Predicting evolution in studies (r)

